PTEP

Prog. Theor. Exp. Phys. **2017**, 12A101 (41 pages)
DOI: 10.1093/ptep/ptx054

Origin of Ultra High Energy Cosmic Rays

Past, present, and future of UHECR observations

B. R. Dawson[1], M. Fukushima[2], and P. Sokolsky[3,*]

[1]*Physics Department, University of Adelaide, Adelaide, Australia*
[2]*Institute for Cosmic Ray Research, University of Tokyo, Kashiwa, Chiba 277-8582, Japan*
[3]*Department of Physics & Astronomy, University of Utah, Salt Lake City, Utah, USA*
[*]E-mail: ps@cosmic.utah.edu

Received February 7, 2017; Revised March 31, 2017; Accepted April 1, 2017; Published November 29, 2017

Great advances have been made in the study of ultra-high energy cosmic rays (UHECR) in the past 2 decades. These include the discovery of the spectral cut-off near 5×10^{19} eV and complex structure at lower energies, as well as increasingly precise information about the composition of cosmic rays as a function of energy. Important improvements in techniques, including extensive surface detector arrays and high resolution air fluorescence detectors, have been instrumental in facilitating this progress. We discuss the status of the field, including the open questions about the nature of spectral structure, systematic issues related to our understanding of composition, and emerging evidence for anisotropy at the highest energies. We review prospects for upgraded and future observatories including Telescope Array, Pierre Auger, and JEM-EUSO, as well as other space-based proposals, and discuss promising new technologies based on radio emission from extensive air showers produced by UHECR.

Subject Index F00, F02, F03

1. Introduction

Cosmic rays were discovered a little over 100 years ago (Refs. [1,2]). They were called "cosmic" to distinguish them from the then equally mysterious "X-rays" emanating from laboratory instruments and particular minerals. The increase in intensity of this cosmic radiation with altitude made it clear that the sources were extraterrestrial. Over the next few decades, grand questions were developed about their origin, the extent of the energy spectrum, and their composition. It took close to 100 years to find the end of the remarkable, approximately power-law energy spectrum, at energies near 50 J per nucleus.

We now know a great deal more, and at lower energies in significant detail (as in the isotopic composition and gamma/electron/positron fluxes). But at the "frontier" energies of $>10^{18}$ eV, where the flux is most likely extragalactic, the experimental tools, while greatly improved, are still too imprecise. While our ability to measure energy with reasonable certitude has improved dramatically, we attempt to measure the cosmic ray composition with what is effectively a blunt instrument. The measurement of arrival directions has also improved markedly, but there, Nature has been unkind and only hints of cosmic ray anisotropy and sources have appeared.

One hundred years ago, the argument was whether the radiation came from the Earth or from space, whether it was composed of charged or neutral particles, and what could be inferred about its energy by measuring "penetrating power". Now the arguments relate to the nature of observed

structures in the energy spectrum—the knees, ankles, and final cut-off, whether the composition is protonic, a mixture of p, He, and CNO group nuclei, or significantly heavy up to Fe, and how this interplays with the spectral structure. Hints of departure from arrival direction isotropy come and go and we fervently hold on to the most recent observation hoping that this time the significance will strengthen with additional data and a source, or sources, will finally be found. But except for the spectrum and its structures, much of what we argue about is ephemeral and can easily change with modification of hadronic models or a decrease in statistical significance of a source. It is a hard fact that we still do not know with any real certainty the origin of cosmic rays above a few tens of gigaelectronvolts in energy. What is it then that we do know, how well, and what are the implications? This is what will be discussed at length in this article. Our knowledge of our deficiencies also leads to new ideas for better detectors and new programmatic approaches to fill in needed extrapolations from accelerator data and ancillary measurements. This too will be explored in subsequent pages.

In the present paper we address broadly the experimental status above 10^{18} eV and briefly describe the current status and the evolution of ultra-high energy (UHE) detection techniques. The pioneering Volcano Ranch, Haverah Park, SUGAR, Yakutsk, and Akeno arrays (Refs. [3–9]) led to the major leaps forward represented by the AGASA, Fly's Eye, HiRes, Auger, and TA experiments (Refs. [9–14]). The early detectors led us to more precise formulations of the questions we now ask. The decades-long development of these second and third generation detectors culminated in the reliable results with well-understood energy and geometrical resolution that have given us new hope that many of the puzzles presented by UHE cosmic rays may soon be answered. The current generation of detectors has brought definitive confirmation on hints of an ankle structure above 10^{17} eV (Ref. [15]) and settled once and for all the reality of a cut-off at energies between 4 and 6×10^{19} eV (Refs. [16,17]). The "holy grail" of UHE cosmic ray physics has been found. It is striking that the suppression is in the same range of energy as the prediction of the Greisen–Zatsepin–Kuzmin (GZK) effect (Refs. [18,19]) (depending somewhat on the assumed distribution of sources, composition and the injection spectrum).

Improvements in the determination of extensive air shower (EAS) profiles and the depth of shower maximum, $X_{\rm max}$, brought about by either using stereo air fluorescence measurements (HiRes and TA; Refs. [20–22]) or by hybrid surface detector and air fluorescence measurements (Auger and TA; Refs. [23–27]) have reduced the reconstruction uncertainties in $X_{\rm max}$ to near $10\,{\rm g\,cm^{-2}}$ with systematic uncertainties approaching this number. We have reached the point where the experimental measurements are becoming more precise than the theoretical underpinnings of the shower simulations used to extract composition information. While data from the LHC in the forward region at an equivalent energy of 10^{17} eV are very helpful in tuning the various hadronic models (Refs. [28,29]), there are significant issues in extrapolating to p-nucleus and nucleus–nucleus interactions at much higher energies (10^{18}–10^{20} eV; Ref. [29]). Currently the combined systematic uncertainties for data and simulations make it difficult to reliably find the mix of protons, He, CNO, and Fe that would match the observed $X_{\rm max}$ distributions. What can be said, and this is a great accomplishment, is that there is very little iron nucleus component (Refs. [25,30]). Why this should be the case, given the relative stability of the iron nucleus as it travels through the relic photon fields, and its relatively high acceleration efficiency, is a puzzle that we are just now beginning to confront.

2. Achievements in the era of very large observatories

2.1. The previous generation of detectors

At the beginning of the 21st century, 3 experiments were studying the highest-energy cosmic rays: the Yakutsk array, the Akeno Giant Air Shower Array (AGASA), and the High Resolution Fly's Eye (HiRes).

The Yakutsk array in Russia has operated in various forms since 1967, and had reached a maximum collecting area of 17 km^2 around 1990. Subsequently, it was reconfigured to study lower-energy cosmic rays, and today it has an area of 8 km^2. While its focus has changed, analyses are still done on the data from high-energy showers already collected, e.g., Ref. [31].

AGASA, located 100 km west of Tokyo at an average altitude of 667 m, operated from 1990 to 2004 as a 100 km^2 array consisting of over 100 scintillator detectors interconnected by optical fibers for timing measurements and data collection (Ref. [32]). It pioneered many of the techniques employed today in more modern observatories, and produced important results on the UHECR energy spectrum, anisotropy, and mass composition (Ref. [33]). Of particular historical interest was the observation by AGASA of the continuation of the cosmic ray spectrum beyond 10^{20} eV, with no sign of a flux suppression (Ref. [34]).

HiRes was the successor to the first successful air fluorescence detector, the Fly's Eye (Refs. [11, 35]), which operated from 1981 to 1993 at the Dugway Proving Grounds in Utah, USA. The Fly's Eye achieved a time-averaged aperture of about 100 km^2 sr at the highest energies, taking into account that it operated only on clear, moonless nights. HiRes was an advancement in resolution and sensitivity, achieved by increasing the telescope effective mirror areas to 3.8 m^2, and reducing the camera pixel angular diameters to 1° (Ref. [36]). Two sites, 12.8 km apart, were instrumented, allowing for stereo observations of approximately 30–40% of air showers that triggered either detector near 10^{19} eV. The collecting area of HiRes was close to an order of magnitude larger than that of the Fly's Eye. The first HiRes site at Five Mile Hill began full operation in 1997, followed by the Camel's Back Mountain site in 1999. HiRes ceased operations in 2006. A summary of the important physics results from HiRes is given in Ref. [14]. This includes the first unambiguous detection of a flux suppression at the highest energies, using monocular data from HiRes I and published in 2008 (Ref. [16]).

At the beginning of the 1990s, discussions began about the next step in UHE cosmic ray observations, where it was recognized that apertures even larger than that of HiRes would be necessary to answer some of the long-standing questions in cosmic ray astrophysics. The experimental challenge was enhanced by the apparent disagreement in the energy spectra presented by AGASA and HiRes in the first few years of the new century. This led to the next generation of experiments adopting hybrid designs, with combinations of surface arrays and air fluorescence detectors.

2.2. Currently operating observatories

2.2.1. The Pierre Auger Observatory

The Pierre Auger Observatory had its beginnings in 1991 when James Cronin and Alan Watson began discussions with a number of experimenters in the field. Its design evolved through an initial meeting in Paris in 1992, a 2-week design workshop in Adelaide in 1993, and a 6-month design study hosted by Fermilab in 1995. Initial ideas were based on a 5000 km^2 surface array without fluorescence telescopes, but the advantages of the hybrid approach soon became apparent (Refs. [39–41]). The Auger Observatory is near Malargüe, Argentina, and its construction began in 2001 with

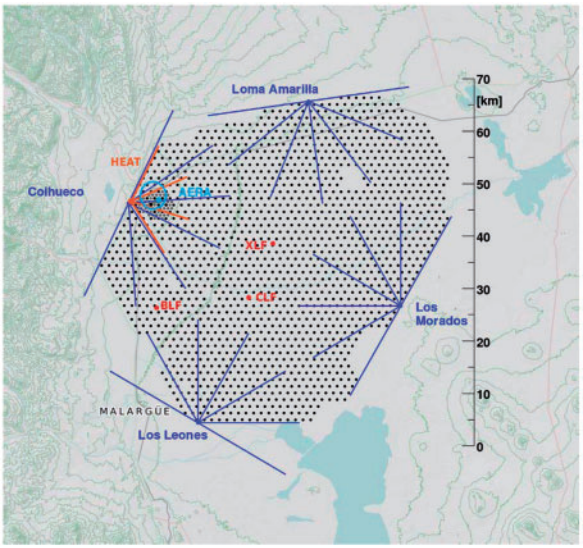

Fig. 1. Layout of the Pierre Auger Observatory, showing the positions of the 1660 SD stations, the fields of view of the main FD telescopes (in blue), and the fields of view of the HEAT high-elevation telescopes (in red). For further details see Ref. [37].

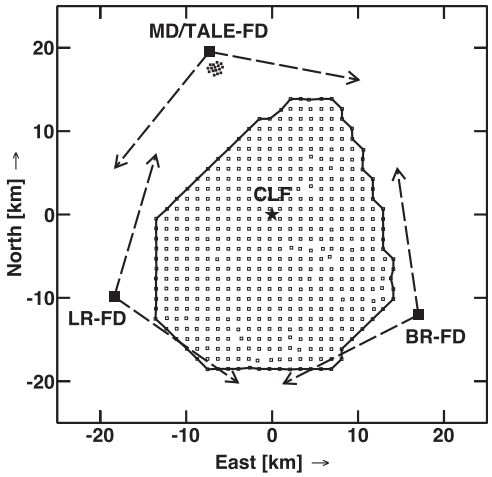

Fig. 2. The Telescope Array layout, showing the locations of the 507 surface detectors. The 3 FD stations at Middle Drum, Black Rock Mesa, and Long Ridge are indicated, each having an azimuthal field of view of about 110°. The TALE detector is situated at the MD site (Ref. [38]).

an engineering array. The observatory was completed in 2008, though official data taking began in 2004 during construction.

Auger's surface detector (SD) consists of 1660 water-Cherenkov detectors (WCDs) arranged on a 1.5 km triangular grid covering 3000 km^2 (Ref. [37]); see Fig. 1. The WCDs are 10 m^2 in area and 1.2 m deep, and build on the experience gained from the Haverah Park detector in the UK (see Ref. [2]). Such detectors have the advantage of having a broad zenith angle sensitivity, and are deep enough to produce signal from the numerous photons in the extensive air shower. The SD is fully efficient for cosmic ray energies greater than 3×10^{18} eV and zenith angles less than 60°. A small 23.5 km^2 area of the array hosts a denser 750 m spacing of WCDs, which is fully efficient for $E > 3 \times 10^{17}$ eV and zenith angles less than 55°.

The main fluorescence detector (FD) consists of 4 sites on the perimeter of the surface array. Each site hosts 6 telescopes, each with a field of view of 30° in azimuth and an elevation range from 1.5° to 30°. Each telescope is of the Schmidt design and consists of a 13 m^2 segmented spherical mirror with a 2.2 m diameter entrance aperture (including a ring of corrector lenses) and a camera composed of 440 photomultiplier pixels, each viewing a 1.5° diameter area of sky (Ref. [37]). The entrance aperture also contains a UV transmitting filter to match the air fluorescence spectrum spanning approximately 300–400 nm. The telescope design benefits from experience with the Fly's Eye and HiRes experiments, with the primary difference being the Schmidt optics design, allowing for a wide field of view with minimal coma aberration. Apart from the 24 telescopes of the main FD described here, an additional 3 telescopes make up the HEAT (High Elevation Auger Telescopes) system. These view the elevation range between 30° and 58° to study lower-energy air showers (currently down to 10^{17} eV) that, due to their lower brightness, are observed closer to the FD site (Ref. [37]).

The combination of the surface and fluorescence detectors to make a "hybrid" observatory has been exploited in much of Auger's scientific output. The SD has many strengths, including robust WCDs that operate with a 100% duty cycle. It also measures the lateral characteristics of the air shower, albeit at one altitude, which are being used for several studies including mass composition. The FD, while having the disadvantage of a 15% duty cycle (Ref. [37]), measures fluorescence light that is produced in direct proportion to the energy deposited by the air shower. Thus, the fluorescence technique measures air shower energies calorimetrically, and it is the FD measurements of energy that calibrate the SD energy scale, as described below. The FD views the developing shower and has access to the depth of shower maximum, $X_{\rm max}$, used in mass composition studies. Finally, the FD reconstruction of the direction and position of the air shower axis is greatly assisted by the SD measurement of the shower arrival time at ground level (Ref. [41]). This hybrid reconstruction produces an FD arrival direction resolution of about 0.5° (Ref. [42]), which helps achieve typical resolutions in energy and $X_{\rm max}$ of $\sim$10% and 20 g cm^{-2}, respectively, at 10^{19} eV (Ref. [43]).

Descriptions of the calibration procedures for both the SD and FD are given in Ref. [37]. In both cases the calibration is "end-to-end", either using unaccompanied muons (in the case of the SD) or a large "drum" to illuminate an FD aperture, so as to calibrate the full detector and data acquisition chain in one step. The atmosphere is also carefully monitored. The density of the lower atmosphere has a well-known effect on the lateral distribution of the air shower at ground level, and these weather corrections are applied to the SD energy measurements for certain studies, such as large-scale anisotropy measurements (Ref. [44]). Finally, the light attenuation characteristics of the atmosphere are measured on an hourly basis during FD operations to account for varying molecular and aerosol scattering, and to monitor cloud cover (Ref. [45]).

The Auger Collaboration had always planned to build a northern array in order to achieve full-sky coverage. The site was chosen to be in south-eastern Colorado, USA (Ref. [46]). Currently there is a strong focus on an upgrade of the southern site (Ref. [47]) (discussed in Sect. 4), and exploration of the northern sky is being undertaken by the Telescope Array Collaboration.

2.2.2. The Telescope Array

The Telescope Array (TA) project was originally proposed around 1997 by members of the AGASA and HiRes experiments as a large fluorescence telescope complex with an effective aperture (after accounting for a 10% duty factor) of 5000 km^2 sr for 10^{20} eV cosmic ray particles (Refs. [48–50]). An apparent discrepancy in the measurements of the UHECR flux above the GZK energy by AGASA and HiRes (see Refs. [16,34]), however, encouraged the members of TA to make a critical examination of

the experimental methods used. This led to the present form of TA, started in 2003, as 2 complete and co-sited SD and FD detectors, each observing the same UHECR events and allowing for a critical comparison of the measured shower parameters (Ref. [51]). The TA experiment occupies a large area near the town of Delta, 200 km south-west of Salt Lake City, Utah, USA, and is now operated by a collaboration of 120 members from 5 countries: Japan, USA, Korea, Russia, and Belgium. The experiment is conducting a high-statistics exploration of the northern sky as a hybrid array of surface and fluorescence detectors.

The TA surface detector comprises 507 detectors on a 1.2 km square grid covering an area of 700 km^2 (Fig. 2). Each detector has an area of 3 m^2 and consists of 2 layers of 1.2 cm plastic scintillator separated by a 1 mm thickness of stainless steel (Ref. [52]). The scintillators are equally sensitive to all minimum ionizing charged particles ($e^{\pm}$, $\mu^{\pm}$), with the SD energy determination being dominated by the EM (electromagnetic) component. This is seen as an advantage as it reduces uncertainties in the energy scale due to mass composition or hadronic physics. The array reaches full efficiency above 10^{19} eV for zenith angles less than 45°, providing an aperture of 1100 km^2 sr.

Three fluorescence detector sites sit near the boundary of the array. One of the sites, at Middle Drum, uses 14 refurbished telescopes originally part of the HiRes detector. They are arranged in 2 "rings" that together view an elevation range from 3° to 31°, and an azimuth range of 112°. Each telescope consists of a 2 m diameter spherical mirror and a camera of 256 hexagonal pixels, with pixels viewing approximately a 1° diameter section of the sky (Ref. [36]).

The other 2 FD sites at Black Rock Mesa (BR) and Long Ridge (LR) each contains 12 newly fabricated telescopes. Each telescope consists of a 3.3 m diameter segmented spherical mirror focusing light onto a 256 pixel camera. The pixels also have a field of view of 1° diameter and each site covers a field of view of 3°–33° in elevation and 108° in azimuth using a 2-ring structure (Ref. [53]). The electronics in the new FD stations digitize the pixel signals at 10 MHz with 14 bits of precision (Ref. [54]).

The TA detectors began full operation in March 2008. Various data sets are being collected, and the consistency between different data sets and different analysis procedures has been carefully examined. Surface detector energy spectrum studies use contained events within the array with zenith angles $<45°$, while anisotropy studies use looser cuts and zenith angles $<55°$ (Ref. [55]). For fluorescence analysis, some studies are done with mono observations (requiring observations from 1 FD site), stereo observations (2 FD sites), and hybrid observations. In the latter case, FD observations are coupled with SD measurements of the shower at ground level, much in the style of Auger analysis, except that timing information from more than 1 SD station is used, and the shower core location derived from SD data alone is used to constrain the hybrid core (Ref. [25]).

The atmospheric transparency of the TA site is monitored by a suite of instruments, including a Central Laser Facility, IR cloud cameras, and a LIDAR station (Refs. [56,57]). In analyses performed to this point, the aerosol content of the atmosphere has been assumed to be constant with time. Atmospheric transparency data has been used to determine an average value of the vertical aerosol optical depth of 0.04 (see, e.g., Ref. [25]), and the effect on systematic uncertainties of fluctuations about the mean has been studied.

The TA project has in recent years extended its reach towards lower-energy cosmic rays with the TALE (TA Low Energy) extension. With an additional 10 telescopes in an extra 2 "rings" at the Middle Drum site, the field of view there is now 3°–59° in elevation and approximately 120° in azimuth. By using Cherenkov-rich events, the energy threshold of TALE is below 10^{16} eV, complementary to

the standard fluorescence observations (Ref. [58]). The surface detector array is being increased in density in front of this FD site to assist with lower-energy hybrid observations.

2.3. Advances in techniques

The advances in our understanding of UHECR that we will discuss in the following sections owe much to the large collecting areas now instrumented by the Auger and TA Collaborations. Additionally, the number of scientists now studying UHECR is much larger than in early generations of experiments, meaning that more manpower is available for the maintenance of the experiments, for calibration of the detectors and the atmosphere, and for devising new and creative analysis techniques and cross-checks. Thus the increase in sensitivity of the modern observatories is due to more than an increase in the collecting area alone. We give some examples here of recently exploited advances in detectors, tools, and techniques.

A stable surface detector is necessary for optimal energy resolution, and for searching for weak broad-scale anisotropies. For example, temperature-dependent particle density measurements can introduce diurnal variations into shower rates above some energy threshold, which may be wrongly interpreted as sidereal harmonics. Both Auger and TA avoid this by monitoring their SD detector performance on short time scales. This is done by collecting histograms of the fundamental unit used to calibrate SD signals—in the case of TA scintillator detectors, a histogram of integrated charges from $\sim$0.4 million penetrating particles is collected every 10 minutes for each detector (Ref. [52]), while for Auger WCDs, histograms of signals from through-going muons are collected every minute, from which the signal due to a "vertical-equivalent muon" (VEM) can be derived (Ref. [37]). In addition to this basic calibration, Auger also makes a correction (in broad-scale anisotropy studies) for the effect of diurnal atmospheric variations on air shower development. These weather effects make small but significant corrections to the SD energy estimator $S(1000)$ (the detector signal 1000 m from the shower core) using the local air density and pressure (Ref. [44]).

In fluorescence light detection, both collaborations have benefitted from experience with the HiRes and Fly's Eye experiments. The electronics in the new FDs in both TA (Ref. [53]) and Auger (Ref. [37]) include sophisticated triggering circuitry, and digitization of each pixel signal is performed at 10 MHz. Improved telescope design is a feature in both experiments, with Auger using a Schmidt optics design that gives a coma-free optical spot over a 30° field of view (Ref. [37]). At TA, signals from UV-bright stars are used to verify ray-tracing estimations of optical aberrations, and to check telescope alignment (Ref. [53]). Calibrations of the FDs feature end-to-end procedures. At Auger, a "drum" calibrating system is moved from telescope to telescope periodically. It uniformly illuminates the aperture of a telescope with an absolutely calibrated light source at a number of wavelengths. Between these absolute drum calibrations, the system calibration is monitored with light sources illuminating the mirror and camera (Ref. [37]). At TA, a small number of absolutely calibrated PMTs are in each camera (Ref. [59]), and their gains are monitored with a radioactive source-scintillator YAP unit (Ref. [60]). The other PMTs in the camera are cross-calibrated and monitored every 30 minutes during observation time using a diffuse Xenon light source installed in front of each camera (Ref. [61]). The Telescope Array is going one step further, experimenting at the Black Rock FD station with an electron light source (ELS) that shoots a vertical beam of 40 MeV electrons 100 m from an FD telescope, creating artificial air fluorescence in situ (Ref. [62]). The ELS aims to make an end-to-end calibration of the FD—from energy deposits in the air to the detection of fluorescence light by the telescope (Ref. [63]).

Since both experiments rely on fluorescence measurements to calibrate the SD energy scales, much effort has recently gone into laboratory measurements of the fluorescence efficiency, that fraction of the shower's ionization energy deposit going into light production. After the pioneering work of Bunner, Kakimoto et al., and Nagano et al. (Refs. [64–66]), new measurements include those of the AIRFLY (Ref. [67]) and FLASH (Ref. [68]) experiments. Results include precise measurements of the fluorescence efficiency and spectrum, and the pressure, temperature, and humidity dependence of the light (Ref. [67]). Auger, which uses the AIRFLY results, has been able to reduce the systematic uncertainty in shower energy associated with the fluorescence yield from 14% to 3.6% (Ref. [69]). TA has used the Kakimoto et al. (Ref. [65]) fluorescence yield model, also used by HiRes, for the sake of consistency and continuity. It is now reexamining its energy scale using more contemporary measurements.

Air shower simulations are used in a variety of applications in both experiments, including the extraction of mass composition estimates from air shower development measurements. The CORSIKA three-dimensional shower simulation program (Ref. [70]) is still the most widely used, with other code such as the longitudinal profile simulator CONEX (Ref. [71]) being used in certain applications. The continuing challenge is to improve the implementation of high-energy hadronic interactions in the code. In the last decade, important new constraints on these interactions have come from measurements at the Large Hadron Collider, spawning new hadronic models for CORSIKA and CONEX, including EPOS-LHC (Ref. [72]), QGSJetII-04 (Ref. [73]), and Sibyll 2.3 (Ref. [74]). Information is also moving in the other direction, with cosmic ray experiments like Auger and TA testing certain aspects of these predictions (see Sect. 2.8).

2.4. The energy spectrum of UHECR

The surface detectors of Auger and TA are the "workhorses" of the respective experiments, since they are operational 24 hours per day and contribute the majority of exposure to studies such as the energy spectrum. However, both experiments use their fluorescence detectors to determine the energy scale of their surface detectors, avoiding much of the uncertainty associated with the alternative, air shower simulations. Systematic uncertainties in the energy scale have been derived taking account of uncertainties in detector calibration and stability, atmospheric transmission, fluorescence yield, and reconstruction. For Auger this amounts to a total systematic uncertainty of 14% (Ref. [69]), and for TA 21% (Ref. [75]). Both quoted uncertainties are independent of energy.

The most recent energy spectra were presented in 2015 by Auger (Ref. [76]) and TA (Ref. [38]). The Telescope Array presented a spectrum over 4.5 decades of energy from below 10^{16} eV, combining results from the SD, the 2 Japanese FD sites (monocular reconstruction), and TALE (Fig. 3). At 10^{20} eV the exposure is approximately 6200 km^2 sr yr for the SD and 650 km^2 sr yr for the FDs. A remarkable set of features is present in the combined spectrum, represented by a series of 5 power-law segments. The flux suppression at the highest energies, identified by TA as consistent with the GZK mechanism (Refs. [18,19]), is present above $10^{19.80\pm0.05}$ eV (6.3×10^{19} eV), and the spectral ankle appears at $10^{18.72\pm0.02}$ eV (5.2×10^{18} eV), again consistent with proton interactions with the cosmic microwave background (CMB) (Ref. [77]). At lower energies, TALE detects two other features, a second knee at $10^{17.30\pm0.05}$ eV (2.0×10^{17} eV), and a low-energy ankle at $10^{16.34\pm0.04}$ eV (2.2×10^{16} eV). The systematic uncertainties of the TALE measurements are currently being evaluated.

The latest Auger spectrum (Ref. [76]; Fig. 4) is a combined measurement from the 1500 m-spaced SD (zenith angle $\theta < 80°$), the FDs operating in hybrid mode, and the 750 m-spaced SD ($\theta < 55°$).

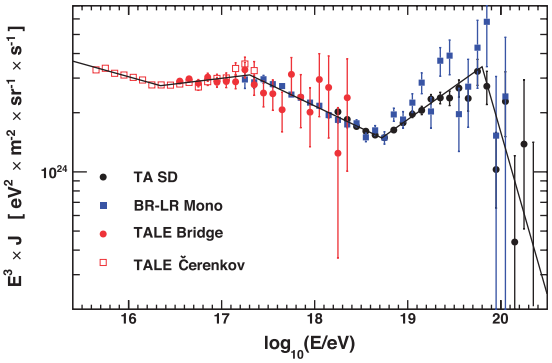

Fig. 3. TA energy spectrum (flux scaled by E^3) with data from TALE, the LR and BR FDs, and the surface detector (Ref. [38]). Five power laws are fitted to indicate the spectral structure. The systematic uncertainty on the energy scale is 21%.

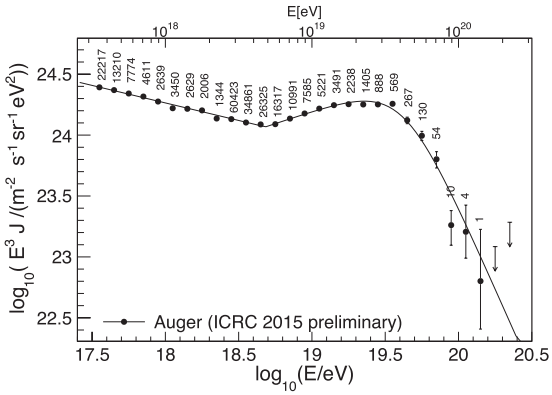

Fig. 4. The Auger combined energy spectrum with data from the 750 m-spaced SD, FD (hybrid), and the 1500 m-spaced SD array. The energy systematic uncertainty is 14%. Event numbers are shown, and a spectrum model is fitted (Ref. [76]).

Two separate analyses were performed for the 1500 m SD array, for "vertical" ($\theta < 60°$) and for "inclined" ($60° < \theta < 80°$) showers, with the latter events being muon dominated. The integrated exposures for the 1500 m vertical SD, inclined SD, and 750 m SD are 42 500 km^2 sr yr, 10 900 km^2 sr yr, and 150 km^2 sr yr, respectively. The energy-dependent exposure for the hybrid spectrum is 1500 km^2 sr yr at 10^{19} eV. The combined spectrum extends from $10^{17.5}$ eV to the highest energies, and shows the ankle feature at $(4.82 \pm 0.07 \pm 0.8) \times 10^{18}$ eV (statistical and systematic uncertainties are quoted). The flux suppression is characterized by a smooth function with $E_s = (4.21 \pm 0.17 \pm 0.76) \times 10^{19}$ eV, with E_s representing the energy at which the flux falls to one-half of the value of the power-law extrapolation.

When comparing the Auger and TA spectra, the following points have been made by a joint Auger/TA energy spectrum working group (Ref. [78]):

- In the overlapping region of energy, the spectral slopes are consistent within uncertainties, and the energy of the "ankle" is consistent given the statistical and systematic uncertainties. A flux difference at energies from $10^{17.5}$–$10^{19.3}$ eV of ∼20% could be the result of a shift in the energy scale within systematic uncertainties.
- On the other hand, the energy of the flux suppression at the highest energies, characterized by $E_{1/2}$ (a measure of the suppression energy favored by TA; Ref. [79]) is inconsistent. The

TA measurement is $(6.0 \pm 0.7(\text{stat})) \times 10^{19}$ eV, compared with the Auger measurement of $(2.47 \pm 0.01(\text{stat})^{+0.82}_{-0.34}(\text{syst})) \times 10^{19}$ eV.

- The agreement in the position of the ankle and the disagreement in the suppression energy might be explained by an energy-dependent systematic uncertainty in energy, or a real difference in the physics of cosmic rays in the northern and southern hemispheres. At the current time, no source of the former has been identified and, as mentioned above, both experiments quote an energy-independent systematic. As an example, differences in the correction for *invisible energy* used by Auger and TA in the FD analyses (i.e., that energy carried by high-energy muons and neutrinos that does not result in proportionate fluorescence light), and differences in fluorescence yield models, produce only a small shift in the energy scale of 5%–10%, which is essentially energy independent.
- The possibility that the UHECR sky is different in the northern and southern hemispheres has been studied by determining the energy spectrum as a function of declination. The Auger SD "vertical" ($\theta < 60°$) spectrum covers a declination range from $-90°$ to $+25°$, 71% of the total sky. Four energy spectra have been derived for independent declination bands (Ref. [76]), which are then compared with the total Auger spectrum. A small, and statistically insignificant, declination dependence in the flux is observed (<5% below the suppression energy E_s and <13% above) within the declinations studied. The conclusion is that the Auger/TA spectrum difference in the suppression region cannot be explained in terms of a declination dependence, unless there is a significant change in the spectrum north of 25°. The TA Collaboration see a hint of such an effect when considering an SD energy spectrum extended to include zenith angles <55°, covering a range of declinations from $-16°$ to $+90°$. The position of the suppression energy $E_{1/2}$ is approximately 3σ higher for declinations north of 26° compared with those south of 26° (Ref. [80]). The question of a declination-dependent spectrum is connected to the observations of anisotropies of the flux discussed below in Sect. 2.5.

Currently the source of the disagreement in the energy spectrum at the highest energies is an open question. Any declination dependence of the spectrum appears weak, but more studies are ongoing. In parallel, the Auger and TA groups are working together to understand differences in the analysis procedures, and how these might lead to an experimental explanation for the spectral differences.

The methods used by the collaborations for measuring the energy spectrum have many things in common, most importantly in the use of fluorescence measurements to set the energy scale. But there are significant differences in other areas, either necessitated by detector differences (scintillators vs water-Cherenkov detectors), or because of the philosophy of the collaborations. A case in point is how each experiment accounts for the zenith-angle-dependent attenuation of showers for SD measurements. The Auger Collaboration has a philosophy of avoiding the use of air shower simulations, wherever possible, in deriving energy estimates. To account for shower attenuation, Auger uses the method of constant intensity cuts (CIC), a data-driven procedure that uses the fact that the intensity of cosmic rays above a certain energy threshold should be independent of the zenith angle of the showers (Ref. [37]). The analysis converts Auger's SD energy estimator $S(1000)$ (the WCD signal 1000 m from the shower core) to S_{38}, the value of $S(1000)$ the shower would have possessed if it had arrived at the median zenith angle of 38°. While, in principle, the conversion from $S(1000)$ to S_{38} could be energy dependent, no dependence has been detected. In contrast, the TA analysis uses simulations of proton showers to account for shower attenuation in their analysis. Both methods are

valid, but both have possible weaknesses, which can be explored in future studies under the joint working group structure created by the two collaborations (Ref. [78]).

The astrophysical interpretation of the energy spectrum is, of course, coupled to other measurements made by the collaborations, in particular the mass composition. The TA Collaboration finds that features of its spectrum can be satisfactorily explained by models of production and propagation of a pure protonic cosmic ray flux (Ref. [81]). Here, the ankle is interpreted as a "dip" caused by pair production on the CMB and IR photons, and the suppression is due to the classic Greisen–Zatsepin–Kuzmin photo-pion production on the same photon fields. Propagation simulations for both a uniform distribution of proton sources, and a distribution that follows the local large-scale structure of the universe, are compared with the measured spectrum to fit the power-law index γ of the spectrum at the sources, a parameter m related to the source evolution with redshift, and a logarithmic shift of the experimental energy scale $\Delta \log E$. Good fits were obtained for both source distributions. For the uniform distribution, the χ^2/d.o.f. was 12.4/17 with $\gamma = 2.21^{+0.10}_{-0.15}$, $m = 6.7^{+1.7}_{-1.4}$, and $\Delta \log E = 0.03 \pm 0.03$ (Ref. [81]). The assumption of the pure proton flux is consistent with TA's measurements of mass composition (see Sect. 2.6). The best value of energy shift (∼3%) is well within the systematic energy uncertainty of TA. The parameters γ and m apply only for sources with $z < 0.7$, since the contribution of protons arriving from sources beyond that redshift is negligible for $E > 10^{18.2}$ eV.

Such a mass composition is not favored by Auger's measurements. In this case it is necessary to use source production and propagation modeling to fit both the energy spectrum, and the mass composition measured at Earth. This has been done by several authors, including the Auger Collaboration (Ref. [82]). The input to the simulation is a population of uniformly distributed sources accelerating protons, and nuclei of He, N, and Fe, to a maximum rigidity with a power-law spectrum of index γ. The standard interactions of protons and nuclei with background photons are taken into account. The result of this simple model is a rather hard input spectrum ($\gamma \sim 1$) with a rather low maximum rigidity of the source accelerators. While the authors point out the naivety of the model, the results are in real contrast to the protonic model favored by the TA Collaboration, and thus stress the importance of the mass composition assumptions when interpreting the energy spectrum.

2.5. *Arrival direction studies*

As described in Sect. 2.3, improvements in detector size, design, and operations have led to major advances in sensitivity for anisotropy studies. In parallel, new Faraday rotation studies have improved our understanding of cosmic magnetic fields, particularly those within our galaxy and its halo (Refs. [83,84]). While the new observatories have not uncovered the strong anisotropies that had been predicted by some, a number of interesting results have ruled out several scenarios for UHECR sources and propagation.

2.5.1. *Broad-scale anisotropy searches*

Broad-scale anisotropies are often searched for using a harmonic analysis in right ascension (RA), though increasingly more sophisticated multipole analyses are undertaken. Results are challenging to interpret, as they depend not only on the distribution of sources, but also on the distribution (including turbulence) of the galactic and extragalactic magnetic fields, and the magnetic rigidity of the cosmic rays.

One case study is the analysis by the Auger Collaboration using both the 750 m and 1500 m SD arrays, covering energies from around 2×10^{16} eV to the highest energies (Ref. [85]). For most

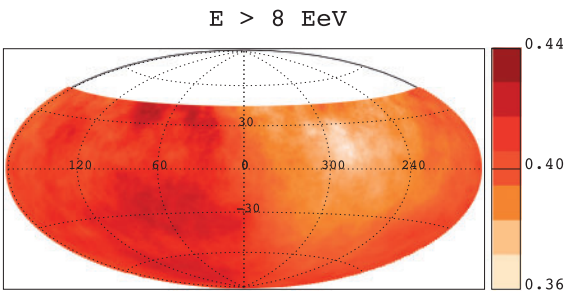

Fig. 5. The Auger skymap (in equatorial coordinates) for $E > 8 \times 10^{18}$ eV. Smoothed over windows of radius 45°, the flux is indicated in units of $\mathrm{km}^{-2}\,\mathrm{sr}^{-1}\,\mathrm{yr}^{-1}$. The significance of the implied dipole is approaching 5σ (Ref. [87]).

of the reported energy range, the amplitude of the first harmonic in RA is not significant, but the phase of the harmonic shows an interesting energy dependence, changing from roughly the Galactic Center direction at low energies to a direction almost 180° away at the highest energies. Linsley pointed out many years ago that the phase information may have some validity even for anisotropy amplitudes that are not significant (see Ref. [86]). Two energy bins have amplitudes approaching acceptable significance—the bin from 1 to 2×10^{18} eV and, especially, the bin for energies above 8×10^{18} eV (Fig. 5). The latter amplitude in RA of 4.4% has a chance probability of 6.4×10^{-5} (Ref. [87]). Expressed as a dipole amplitude and direction, the excess is $7.3 \pm 1.5\%$ (approaching 5σ) in a direction $(\mathrm{RA}, \mathrm{dec}) = (95° \pm 13°, -39° \pm 13°)$.

This apparent transition of the phase of the anisotropy from the Galactic Center direction to the opposite direction coincides in energy with the ankle of the spectrum, an energy range often seen as the transition between galactic and extragalactic sources (e.g., Ref. [89]). It is also an energy where both Auger and TA find that protons seem to dominate the flux (see Sect. 2.6). The *dominance* of protons of *galactic* origin around 10^{18} eV is excluded by the low limits on the amplitude of the anisotropy as measured by both Auger and TA (Refs. [90,91]) with TA concluding that less than 1.3% (95% CL) of cosmic rays with energies between 1 and 3×10^{18} eV are galactic protons (given certain assumptions about the galactic and halo magnetic fields, and assuming an isotropic extragalactic flux). If, in this region, an extragalactic flux is taking over from a galactic origin, the low level of anisotropy could be explained by the flux being the sum of 2 fluxes with first-harmonic phases almost 180° apart.

The Auger and TA Collaborations have combined data to examine broad-scale anisotropies above 10^{19} eV with a full-sky coverage (Refs. [92,93]). Only in such a full-sky analysis can a true dipole moment be measured unambiguously, and higher moments searched for confidently. With the current statistics, a dipole moment of amplitude $6.5 \pm 1.9\%$ is seen with a chance probability of 0.5% and a direction consistent with the Auger-only result above 8×10^{18} eV described above. Future joint analyses are awaited with interest.

2.5.2. Small- and medium-scale anisotropy searches

At the highest energies, source distances are likely to be closer than 100 Mpc because of energy loss interactions of cosmic rays (of all masses) on various photon fields (e.g., Ref. [94]). Then, if magnetic deflections are not too extreme, the arrival direction distribution will mirror the distribution of sources in the local universe. Both collaborations have searched for event clustering, and for

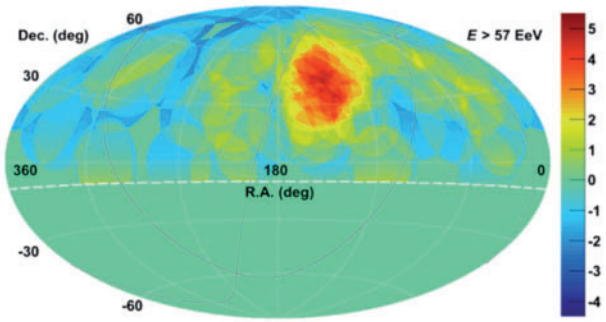

Fig. 6. The TA "hotspot" in 2014 in equatorial coordinates. The number of events observed above 5.7×10^{19} eV within a 20° radius area of sky is 19 when 4.49 are expected, giving a post-trial significance of 3.4σ (Ref. [88]). (The color scale represents σ).

cross-correlations with various astronomical catalogs over a range of angular scales and above a number of energy thresholds.

The most recent Auger data set (including inclined events out to a zenith angle of 80°) has been used for searches with energy thresholds between 4 and 8×10^{19} eV (Ref. [95]). Self-clustering, and clustering around the galactic plane, the Galactic Center, and the supergalactic plane, have been tested. In addition, cross correlation analyses have been performed with catalogs of extragalactic objects. No significant anisotropies were found. Of the studies done, the two with the smallest post-trial probabilities (both 1.4% as it happens) were a correlation of cosmic ray arrival directions ($E > 5.8 \times 10^{19}$ eV) with directions of active galaxies in the Swift-BAT X-ray catalog closer than 130 Mpc and with luminosities greater than 10^{44} erg s^{-1}, using an 18° search radius; and a clustering of cosmic rays above the same energy threshold within a 15° radius of our closest active galaxy, Centaurus A.

The TA Collaboration have done similar searches (Refs. [96,97]) with similar null results. However, an excess on a medium angular scale of 20° radius has been detected above 5.7×10^{19} eV in the direction $(\mathrm{RA}, \mathrm{dec}) = (146.7°, 43.2°)$. With 5 years of TA data, the "hotspot" contained 19 events when the background expectation was 4.49 (Ref. [88]). After accounting for trials, including the choice of angular scale, the significance of the excess is 3.4σ (Fig. 6). There is no obvious source or galaxy cluster in this direction, though the excess may be associated with large-scale structure, its center being 19° away from the supergalactic plane. An update of the result with an additional 2 years of exposure showed a total of 24 events when the background expectation was 6.88 (Ref. [98]). This represents a 3.4σ post-trial significance, no change since the original result. The future evolution of this analysis will be followed with interest.

The lack of strong statistical evidence for small-scale anisotropies at the highest energies starts to put constraints on the source characteristics, but those constraints are tightly coupled to the mass (charge) of the particles and the magnetic fields. If the UHECR were proton dominated, and if extragalactic magnetic fields were generally at the nano-gauss scale, we would need to conclude that there was a high source density within the 100 Mpc horizon (e.g., Ref. [99]). On the other hand, if most of the UHECR have medium to high charge, the lack of strong anisotropy could be blamed on magnetic deflections. This emphasizes the importance of the next topic in our discussion.

2.6. Interpretations of mass composition from air shower measurements

Unfortunately our access to information on the mass of UHECR is rather indirect, through observations of the extensive air showers they initiate. We must rely on models of hadronic interactions at

extreme energies to interpret these observations in terms of the mass of the cosmic ray. As described in Sect. 2.3, hadronic models have improved in recent years with the availability of measurements from the LHC at center of mass energies of up to 13 TeV. However, given that this corresponds to a fixed target energy of around 10^{17} eV, laboratory measurements still fall short of the energies involved in UHECR interactions.

With this large caveat in mind, we can attempt to transform measurements of air shower development into estimates of primary mass.

2.6.1. Fluorescence detector measurements of shower depth of maximum

For many years, the depth of shower maximum $X_{\rm max}$ has been the prime measurement for this purpose, first in Cherenkov light experiments around the knee of the energy spectrum in the 1970s, and more recently in fluorescence detector measurements at the highest energies. The quantity $X_{\rm max}$ is the slant depth in the atmosphere (in g cm^{-2}) at which the air shower reaches its maximum size (number of particles) or, near equivalently, at which the shower reaches the maximum of its energy deposit, dE/dX. From simple arguments it can be shown that the depth of maximum increases with the logarithm of the primary energy for a fixed primary mass, and with the logarithm of the primary mass number, A, at fixed energy (e.g., Ref. [100]).

Unprecedented resolution in $X_{\rm max}$ is now possible with the fluorescence technique, particularly due to reliable reconstruction of the shower axis with the hybrid or stereo techniques, and partly due to finer pixelization and digitization in FD cameras. Statistical resolution can be better than 20 g cm^{-2} above 10^{19} eV (Refs. [27,101]), with measurement systematics below 10 g cm^{-2} for Auger (Ref. [27]) and somewhat higher for TA (Ref. [25]). Now it is possible to confidently quote not only mean values of $X_{\rm max}$ as a function of energy, but also the width (RMS or σ) of the distribution in some energy range.

In the interpretation of $X_{\rm max}$ measurements, one needs to be aware of any biases imposed by the detection or reconstruction processes. A simple example of detection bias would be a bias against the detection of showers with very deep $X_{\rm max}$ (say 900 g cm^{-2}), since vertical showers of this type would have their maxima very close to, or below, ground level. The Auger and TA Collaborations have approached the detection bias issue in quite different ways, both valid. The Auger approach (Ref. [27]) is to apply strict cuts on the axis geometry of air showers to avoid bias in the detection of both shallow and deep showers. Despite the cost of lower statistics, this allows evaluation of the energy dependence of the "true" (free of detector bias) $X_{\rm max}$ distributions, which can then be compared with theoretical predictions for various mass groups. When computing the RMS of the $X_{\rm max}$ distributions, the experimental resolution is subtracted in quadrature, and care is taken (with more than one method) to account for possible undersampling of the tails of the distributions (Ref. [27]).

The alternate philosophy, practised by TA (Ref. [102]) and inherited from the Fly's Eye and HiRes approaches, is to apply cuts based only on data quality, not potential bias. The theoretical expectation for a particular mass group is then derived using simulations of the detection and reconstruction processes, so that any biases and resolution effects are also present in the expectation. This procedure maximizes the event statistics for analysis. However, the results are not *easily* comparable with measurements from other detectors.

The Auger Collaboration has presented results on both the mean and RMS of $X_{\rm max}$ ($\langle X_{\rm max}\rangle$ and $\sigma(X_{\rm max})$) from 10^{17} to $10^{19.6}$ eV (Ref. [103]), as shown in Fig. 7. The reduction in the lower energy

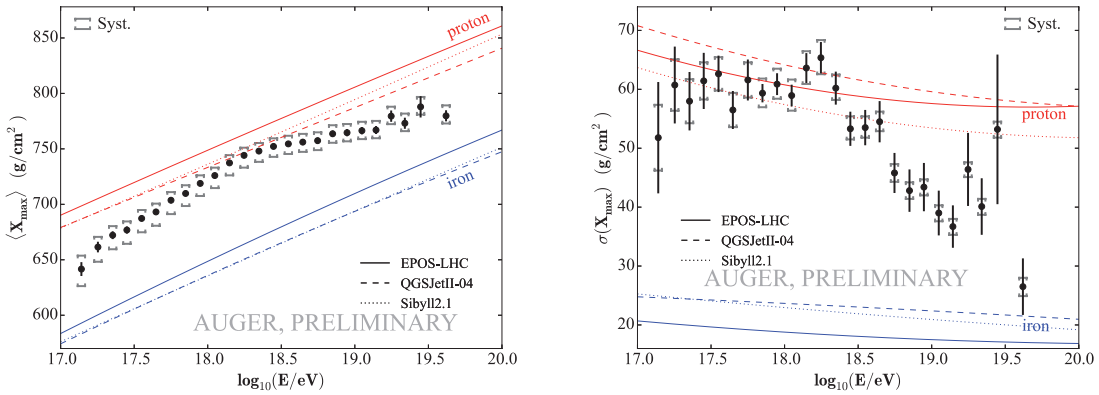

Fig. 7. Auger results on the mean X_{max} (left) and its RMS (right), compared with expectations for protons and iron using the EPOS-LHC, QGSJetII-04, and Sibyll 2.1 hadronic models. Statistical and systematic error bars are indicated (Ref. [103]).

limit below the previous value of $10^{17.8}$ eV (Ref. [27]) is due to the inclusion of data from the HEAT FD enhancement (see Sect. 2.2.1). The number of events in the latest analysis is 23 872, including 7142 events above $10^{18.2}$ eV. The results can be summarized as follows:

- The rate of change of $\langle X_{max} \rangle$ per decade of energy (known as the elongation rate) is not consistent, at any energy, with that expected of an unchanging mass composition, namely about 60 g cm^{-2} per decade. Below $10^{18.3}$ eV the elongation rate is 85 g cm^{-2} per decade, while above that energy it becomes much flatter at approximately 26 g cm^{-2} per decade. This is interpreted as the average mass of cosmic rays decreasing with energy up to the breakpoint, and then increasing again up to the highest energies. (The lower energy elongation rate is compatible with the measurement by the HiRes/MIA experiments in the same energy range; Ref. [23]).
- The behavior of $\sigma(X_{max})$ is broadly consistent with the behavior of the mean value. Up to $10^{18.3}$ eV the spread of X_{max} is roughly constant (plausible even if the mean mass is decreasing, since a significant proton component appears to remain throughout this energy range), after which the spread appears to decrease with energy.
- Using 2 post-LHC hadronic models, EPOS-LHC and QGSJetII-04, the experimental data are expressed in terms of $\langle \ln A \rangle$ and $\sigma^2(\ln A)$, where A is the mass number of a cosmic ray nucleus (Ref. [27]). With both models, the mean value of A is similar at the lowest and at the highest energies explored, while reducing to a minimum at around $10^{18.3}$ eV. The EPOS-LHC model interprets the data with a slightly heavier mean A at all energies, compared with QGSJetII-04. At the higher energies, $\sigma^2(\ln A)$ approaches zero for the EPOS-LHC model (implying a single type of nucleus) and becomes unphysically negative for the QGSJetII-04 model.
- The X_{max} distributions for energy bins from $10^{17.8}$ eV to the highest energies have been fitted with model expectations for mixtures of protons with nuclei of helium, nitrogen, and iron (Ref. [30]). With the current models, a simple mixture of protons and iron is not a good fit at any energy, but acceptable fits are obtained when intermediate masses are introduced. For all models, there is a significant reduction in the proton fraction with increasing energy above $10^{18.3}$ eV, and no model requires any significant fraction of iron at any energy. However, the intermediate masses concluded to be present at any energy have a strong model dependence.

Despite the interpretational problems associated with hadronic physics models, the Auger results show a clear structure in the evolution with energy of both $\langle X_{\rm max}\rangle$ and $\sigma(X_{\rm max})$. The data do not appear consistent with a mass composition unchanging with energy.

In the past 3 years the TA Collaboration have discussed the results of 3 $X_{\rm max}$ analyses, all using the previously discussed philosophy of maximizing statistics by applying only data quality cuts. Detection biases are accounted for by comparing real data with simulations having the same biases. Those analyses are a hybrid study of data from the Middle Drum (MD) FD detector using 5 years (Ref. [25]) and 7 years (Ref. [101]) of exposure; a study of data from all 3 FDs using "stereo" geometrical reconstruction (Ref. [104]); and a recent study of hybrid-reconstructed showers viewed by the Black Rock Mesa and Long Ridge (BR/LR) fluorescence detectors over 7 years (Ref. [101]). We summarize the conclusions of those studies here:

- The MD hybrid study published in early 2015 (Ref. [25]) detailed the analysis of showers with energies above $10^{18.2}$ eV viewed by the refurbished HiRes FD detector over 5 years. Using improved profile reconstruction cuts (based on a pattern recognition approach), $X_{\rm max}$ resolution better than 25 g cm^{-2} was achieved, with a systematic uncertainty in $X_{\rm max}$ of better than 18 g cm^{-2}. Data were compared with expectations of the QGSJetII-03 hadronic model, both in terms of the mean $X_{\rm max}$ as a function of energy, and by comparing the shapes of the $X_{\rm max}$ distributions in a number of energy bins. The overall conclusion was that, taking into account systematic uncertainties, the mean behavior and the distributions are consistent with the expectations for a light, mainly protonic composition. An additional 2 years of hybrid MD data were included in an analysis presented in 2016 (Ref. [101]) with no change in conclusions.
- An alternative to "hybrid" geometrical reconstruction of FD events using information from the SD is to use the stereo technique combining views of the shower from at least 2 FD sites. An $X_{\rm max}$ analysis of stereo data from all 3 FD sites over 7 years was published in 2015 (Ref. [104]), with an energy threshold of $10^{18.4}$ eV. The $X_{\rm max}$ resolution and systematic uncertainty were similar to the MD hybrid analysis above. Comparisons were made with 5 hadronic interaction models, including 2 making use of recent LHC input. The trend is for more recent hadronic models to predict deeper developing air showers. Based on the behavior of the mean $X_{\rm max}$ as a function of energy, and on the shape of the $X_{\rm max}$ distribution for all energies, the authors conclude that no iron is required at any energy, and that the data are consistent with protons from the early QGSJet-01c model. While pure protons from post-LHC models are disfavored, a light composition remains consistent with the data within the systematic uncertainties.
- Finally, a new analysis of 7 years of hybrid data from the BR/LR FD stations was presented at the UHECR 2016 conference (Ref. [101]). This data set is the largest, with 2597 events above $10^{18.2}$ eV, compared with 1346 events from the stereo analysis ($E > 10^{18.4}$ eV) and 623 from the MD hybrid analysis. With the aid of the FADC digitization of the signals in these FD sites, the $X_{\rm max}$ resolution is improved to better than 20 g cm^{-2}, though the systematic uncertainty is now conservatively quoted as 20.3 g cm^{-2}. The data are compared with expectations from the QGSJetII-03 and QGSJetII-04 models; see Fig. 8. One conclusion is that, within the systematic uncertainty, the mean $X_{\rm max}$ vs energy is consistent with that expected for a "light" composition. In addition, the *shapes* of the $X_{\rm max}$ distributions in 5 energy bins are consistent with the protonic expectations, and inconsistent with those of iron.

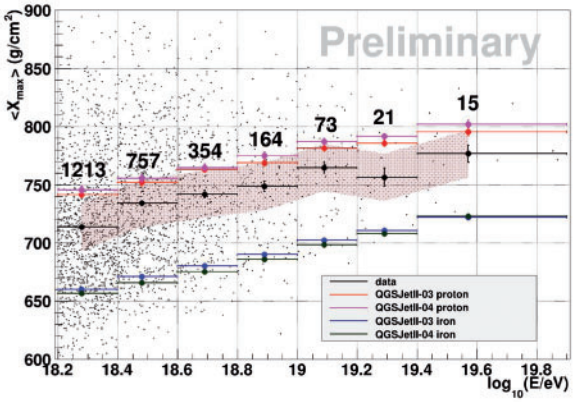

Fig. 8. Telescope Array observed mean $X_{\max}$ results from 7 years of hybrid data from the BR/LR fluorescence detectors (preliminary data). Data are compared with the expectations for protons and iron from the QGSJetII-03 and QGSJetII-04 hadronic models. A systematic uncertainty of 20 g cm^{-2} is indicated by the shaded region (Ref. [101]).

A joint group of collaborators from both Auger and TA have been working to understand the differences in $X_{\max}$ results from HiRes, TA, and Auger (Refs. [105–107]). A particular question is, are the differences related to experimental factors, or due to the interpretation via hadronic models? As we have discussed, the comparisons are complicated by the different philosophies of the experiments, with Auger applying cuts designed to remove detection bias. In their latest report (Ref. [107]), the group has asked the following question: Are the measurements of $X_{\max}$ made by Auger (both the mean values and the distributions) consistent with the measurements of TA? This is a question quite separate from any particular hadronic model and mass interpretation, though such models must be used to "translate" Auger measurements into TA expectations. The Auger fractions of protons and nuclei of He, N, and Fe in energy bins above $10^{18.2}$ eV were taken from Ref. [30] under the assumption of the QGSJetII-04 model. Those mixtures were then processed through the TA detector simulation and reconstruction to give the $X_{\max}$ distributions expected in each energy bin at TA for the Auger "mix", taking into account any detection bias. In particular, the comparison was done for the 7-year, higher-statistics BR/LR hybrid data set described above. The conclusions are that the Auger mix produces a mean $X_{\max}$ as a function of energy that is consistent with the TA measurements within the current systematic uncertainty of 20 g cm^{-2}, and that there is also qualitative agreement between the shapes of the Auger mix distributions of $X_{\max}$ and TA distributions in several energy bins below 10^{19} eV where TA has sufficient statistics. Above 10^{19} eV, the TA data still suffer from insufficient statistics to come to more definite conclusions about the distribution widths. This important study removes much of the doubt about the consistency of Auger and TA results, and shows the importance of continuing dialog between the 2 experiments.

2.6.2. Other mass-related measurements

Surface detector arrays are sensitive to variations in shower development (and hence mass) through measurements of parameters such as the pulse rise-time in a detector, the radius of curvature of the shower front, and the lateral distribution function (e.g., see historical examples in Ref. [3]). Those arrays with particular sensitivity to muons can also attempt to tackle the mass issue through measuring the muon content of air showers, as will be discussed in Sect. 2.8.

Recently the Auger Observatory, in particular, has explored air shower development with several SD methods, and we briefly mention two here. While the resolution in inferred mass-related parameters such as $X_{\rm max}$ is typically poorer than the equivalent FD measurement, the SD has the advantage of a 100% duty cycle.

The rise-time of a signal in a water-Cherenkov detector, defined as the time taken for the signal to increase from 10% to 50% of the total integrated value, is related to the core distance of the WCD and the zenith angle of the air shower. It also displays azimuthal asymmetry with respect to the azimuth of the shower axis, which can be exploited to study shower development (Ref. [108]). The conclusion of the study is that, above $10^{18.5}$ eV, there appears to be an increase in the mean mass of cosmic rays, but that the detail of the mass increase depends on the hadronic model assumed, and the core radius range used in the analysis. The latter dependence implies a deficiency in both of the (post-LHC) hadronic models used.

Similar interpretational issues occur with Auger's measurements of the muon production depth, MPD, using inclined energetic showers above $10^{19.3}$ eV (Refs. [109,110]). In such showers, the electromagnetic component of the shower is essentially absent at ground level, and the digitized signals from the WCDs can be analyzed to give the longitudinal profile of the production depths of muons, and the depth of the maximum of that profile, $X^{\mu}_{\rm max}$. While not the same as the depth of maximum of the overall shower $X_{\rm max}$ (dominated by the electromagnetic component), $X^{\mu}_{\rm max}$ also has sensitivity to mass. The measurements show that the mean $X^{\mu}_{\rm max}$ is effectively flat with energy above $10^{19.3}$ eV, implying a mass increasing with energy. The mean mass implied by the QGSJetII-04 model is heavy, but that implied by the EPOS-LHC model is unphysically heavier than iron. Again, this is an indication that the current hadronic models are not describing the measurements well.

Finally, there is one Auger measurement, this time at energies just above the spectral ankle ($10^{18.5}$–10^{19} eV), where it is claimed that its main conclusion is insensitive to details of hadronic models (Ref. [111]). Here, hybrid data are used to produce a scatterplot of $X_{\rm max}$ vs $S(1000)$, and a correlation coefficient is determined. (The energy and zenith-angle dependencies of the variables are removed before plotting.) The value of the correlation coefficient is found to be inconsistent with any *pure* composition of *any* mass, with the conclusion the same for all 3 post-LHC hadronic models tested. This result disfavors, e.g., a pure protonic cosmic ray flux around the spectral ankle, that proposed by the so-called dip model of this feature (Ref. [77]).

2.7. Photons and neutrinos

Apart from attempting to characterize the nuclei within the cosmic ray flux, there is great interest in searching for photon and neutrino candidates within the events detected by the experiments. Photons and neutrinos will be produced at some level in the sources due to interactions of hadronic cosmic rays with ambient gas and photon fields. They will also be produced through photo-pion production when the highest-energy protons interact with photons of the cosmic microwave background (often called "GZK" or cosmogenic photons and neutrinos; Refs. [112,113]), and several exotic models of "top-down" cosmic ray production (e.g., from super-heavy dark matter) predict significant photon fluxes (e.g., Ref. [114]). Thus measurements, or limits, on the flux of UHE photons and neutrinos are important.

2.7.1. Recent photon limits

Both TA and Auger have produced updates to their photon limits in the past 2 years. For TA, the discrimination between hadronic- and photon-initiated air showers is made using a multivariate

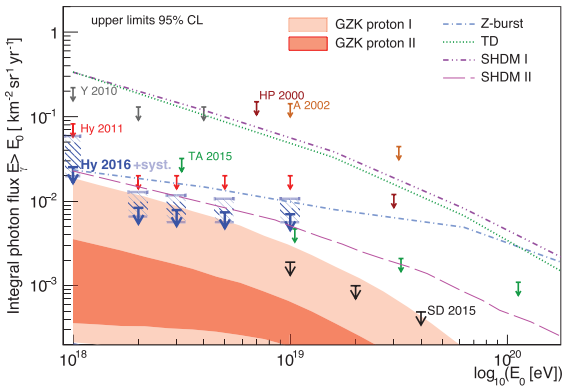

Fig. 9. Diffuse photon integral flux upper limits (95% CL) from Auger (black and blue points; Ref. [115]) and TA (green points; Ref. [116]). For references to the other measurements and the model predictions, see Ref. [115].

analysis of TA SD data using machine learning techniques (Refs. [116,118]). Among the variables tested are a shower-front curvature parameter, and the signals in the top and bottom layers of the SD scintillators, the latter seeking to exploit the deficit of muons in photon-initiated showers. No photon candidates were observed with $\theta < 60°$, and 95% CL upper limits on the integral flux were derived: 0.032, 0.0047, 0.0021, and 0.0011 $\mathrm{km^{-2}\,sr^{-1}\,yr^{-1}}$ above 3, 10, 30, and 100 $\times$ 10^{18} eV respectively.

The Auger Collaboration searches for photons using 2 techniques. At lower energies hybrid data are used, and a multivariate analysis of variables including X_{max} and a measure of the SD lateral distribution function (LDF) is the basis of the photon discrimination (Ref. [115]). Using 9 years of hybrid data, 3 photon candidates have been identified near 10^{18} eV, a number consistent with the expected misclassification of hadronic showers. Thus, upper limits on the integral photon flux are calculated for 5 lower-energy thresholds of 1, 2, 3, 5, and 10 $\times$ 10^{18} eV, namely, 0.027, 0.009, 0.008, 0.008, and 0.007 $\mathrm{km^{-2}\,sr^{-1}\,yr^{-1}}$ (95% CL). This puts the photon fraction of the flux at less than 0.1% in the first bin and less than 2.7% in the last.

In the decade of energy above 10^{19} eV, SD data alone were used in the Auger study (Ref. [119]). There, discriminating shower parameters are related to the signal LDF and to the rise-times of the WCD signals—photon showers have steeper LDFs and longer rise-times than hadronic-initiated showers. With 8.5 years of data, 5 photon candidates are observed (consistent with expectations for hadronic misclassification), and the upper limits on the photon integral flux are $(1.9, 1.0, 0.49) \times 10^{-3}\,\mathrm{km^{-2}\,sr^{-1}\,yr^{-1}}$ (95% CL) above thresholds of 1, 2, and 4 $\times$ 10^{19} eV.

These limits are summarized in Fig. 9. Note that while the Auger results are stronger because of the larger exposure, the TA experiment explores a different hemisphere, relevant in the case of point sources. The figure shows expectations for models of top-down production of UHECR, now disfavored at almost all energies, as are 2 models of cosmogenic photons that assume a pure proton UHECR flux. The experimental limits are encroaching on the cosmogenic model with optimistic selections of the source spectral index and maximum energy. The other model expectation, assuming a proton source spectral index of $\gamma = 2$ and a maximum energy of 10^{21} eV, is 4 times lower than the integral limit at 10^{19} eV. Sensitivity to this model may be reached by the current experiments in the next decade.

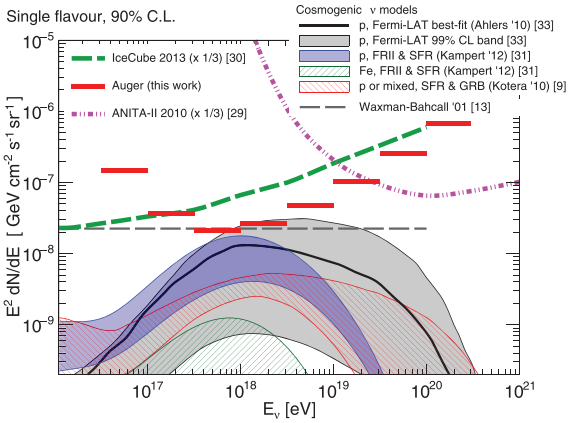

Fig. 10. The Auger single-flavor limits to the UHE neutrino flux (90% CL) in half-decade bins, with the equivalent limits from IceCube and ANITA. For references to these other measurements, and the cosmogenic models shown, see Ref. [117].

2.7.2. Recent neutrino limits

The current competitive limits on UHE neutrinos come from the Pierre Auger Observatory and the IceCube experiment. The Telescope Array has not yet published results of their searches. IceCube and Auger have similar sensitivities at the highest energies.

The basis of Auger's neutrino search is to identify "young" showers at large zenith angles (or indeed, upward-going) in the SD data set. A young shower at ground level is one with both electromagnetic and muonic components intact. The electromagnetic component of a large zenith angle shower initiated by a hadron will be absorbed by the atmosphere before hitting the ground, so "normal" inclined events are characterized by SD station signals with fast rise-times and short durations. Auger's latest limits have combined results from 3 searches to give its most sensitive single-flavor limits to date (Ref. [117]). The searches include 1 for earth-skimming showers (sensitive to ν_τ), and 2 searches in 2 zenith angle bands ($\theta \in (60°, 75°)$ and $\theta \in (75°, 90°)$) sensitive to all 3 flavors. No candidates were identified, and the limits are shown in Fig. 10. These limits are now having some astrophysical significance, with some models of neutrino production in sources, and exotic production mechanisms, being ruled out. In particular, cosmogenic neutrino production models that assume pure proton fluxes at high-redshift sources and strong source evolution (like FR-II galaxies) are highly disfavored by the Auger analysis (Ref. [117]). Similarly, the recent IceCube analysis excludes with a 90% CL proton sources evolving strongly with the evolution parameter $m > 5$ and with redshifts z up to 1.4 (Ref. [120]).

In other neutrino-related studies, the Auger, TA, and IceCube experiments have reported a negative finding on a search for coincident arrival directions of IceCube neutrinos and Auger and TA UHECR (Ref. [121]). The Auger Observatory has also searched for neutrino events associated with the first two LIGO gravitational wave observations (Ref. [122]).

2.8. Interaction cross sections and tests of hadronic physics

As we have seen, modern cosmic ray observatories rely on models of hadronic interactions to interpret shower development measurements in terms of the primary cosmic ray mass. Thankfully, the near-calorimetric fluorescence technique has meant that energy assignments have very little dependence on these models.

Despite the very indirect nature of our observations of cosmic ray interactions, modern observatories can contribute knowledge to the nature of hadronic physics at energies well above those probed by the LHC. Two example areas are measurements of interaction cross sections, and the identification of model deficiencies in predicting ground signals.

2.8.1. The proton–air inelastic cross section at ultra-high energies

The first measurements of $\sigma^{\rm inel}_{\rm p-air}$ using cosmic rays at extreme energies were made by the Akeno (Ref. [123]) and Fly's Eye (Refs. [124,125]) experiments, followed later by HiRes (Ref. [126]). While Akeno showed that this measurement was possible using a surface array (characterizing shower development using electromagnetic and muon content at ground level), the Fly's Eye and subsequent experiments have used FD observations of $X_{\rm max}$. The exponential tail of a histogram of $X_{\rm max}$ measurements is fitted with a function $\exp(-X_{\rm max}/\Lambda)$ to yield the scale of the exponential Λ. Provided the showers contributing to the tail are initiated by protons, Λ can be converted to $\sigma^{\rm inel}_{\rm p-air}$ with a relatively small sensitivity to hadronic interaction models. For comparisons to accelerator data, the inelastic proton–air cross section may be converted to the inelastic and total proton–proton cross sections using Glauber theory (see, e.g., Ref. [127]).

The Auger Collaboration measurements were published in 2012 (Ref. [127]) and updated with increased statistics in 2015 (Ref. [128]). The energy range of interest is around 10^{18} eV where the mass composition appears proton-rich. In the latest analysis, 2 energy bins are used, $10^{17.8}$–10^{18} eV and 10^{18}–$10^{18.5}$ eV, corresponding to center-of-mass energies of 39 and 56 TeV, respectively. Only the deepest 20% of the showers are used in the analysis to minimize contamination from primaries other than protons. Nevertheless, an important systematic uncertainty is related to the possible contamination by helium nuclei. Conservatively, a 25% contamination of helium is assumed. Results for $\sigma^{\rm inel}_{\rm p-air}$ are $[457.5 \pm 17.8({\rm stat})^{+19}_{-25}({\rm syst})]$ mb at 39 TeV and $[485.8 \pm 15.8({\rm stat})^{+19}_{-25}({\rm syst})]$ mb at 56 TeV. Of the total systematic uncertainty, ± 10 mb is attributed to hadronic model sensitivity at both energies.

The recent Telescope Array analysis is of showers observed by the Middle Drum FD detector in hybrid mode (Ref. [129]). Air showers over the energy range from $10^{18.3}$–$10^{19.3}$ eV are used, corresponding to an average center-of-mass energy of 95 TeV. Showers in the tail of the $X_{\rm max}$ distribution beyond 790 g cm^{-2} are assumed to be protons. Assuming a 25% contamination of helium in the tail, $\sigma^{\rm inel}_{\rm p-air}$ is determined to be $[567.0 \pm 70.5({\rm stat})^{+29}_{-25}({\rm syst})]$ mb.

The results from both experiments have been converted to proton–proton cross sections to rule out the more extreme extrapolations of accelerator data (Refs. [127,129]).

2.8.2. Characterization of deficiencies in hadronic models

Both the Auger and Telescope Array experiments have detected likely deficiencies in the hadronic interaction models employed in air shower simulations. That there are deficiencies is unsurprising, given that these models are extrapolations of direct accelerator measurements, but it is encouraging that some of the more recent models, based on LHC data, are less discrepant with respect to the cosmic ray measurements (see below).

An example from the TA experiment relates to the SD energy estimator $S(800)$. It has been related to primary energy using simulations of proton showers (a preference based on HiRes and TA interpretations of mass composition) and the QGSJetII-03 hadronic model (Ref. [130]). The SD energy ($E_{\rm SD}$) at a given zenith angle is determined as the (simulation) energy that reproduces the measured $S(800)$ at the same zenith angle. For hybrid events, the ratio $E_{\rm SD}/E_{\rm FD}$ is found to be 1.27,

where $E_{\rm FD}$, the FD energy, is obtained calorimetrically and is essentially free of hadronic physics uncertainties. The ratio has no significant dependence on energy or zenith angle for $E > 10^{18.5}$ eV and $\theta < 45°$. The lateral distribution and other experimentally measured variables are well reproduced by the energy-rescaled shower simulation (proton, QGSJetII-03). The required rescaling points to a deficiency in the simulations that predicts fewer charged particles (electrons and/or muons) hitting the SD, although a further quantitative analysis studying the dependence on hadronic model, assumed mass composition, and zenith angle is necessary. The uncertainty of the ratio $E_{\rm SD}/E_{\rm FD}$ is currently dominated by the FD energy uncertainty, which is 21% for TA, and its improvement will help to pin down the nature and the level of the deficiency.

The Auger Collaboration has studied the muon content of inclined (zenith angle 62°–80°) air showers above 4×10^{18} eV (Ref. [131]). At these angles the electromagnetic component of the showers is absorbed by the atmosphere, and the WCD signal is essentially due to muons. Using hybrid showers, the energy is known from the FD (to within its systematic uncertainty of 14%) and the muon content measured by the SD can be compared with expectations from simulations (using 2 pre-LHC and 2 post-LHC hadronic models) of proton, iron, and mixed compositions. The mixed composition is that implied (for each hadronic model) from Auger FD measurements at these energies. A relative integrated muon number R_μ, designed to remove the energy and zenith-angle dependencies of the measurement, is used to compare real measurements with simulations. It is found that the simulations underestimate the muon measurements by $(30^{+17}_{-20}(\text{syst}))\%$ to $(80^{+17}_{-20}(\text{syst}))\%$ for the assumed mixed composition at 10^{19} eV, over the range of models tested. The models with smallest discrepancy are the post-LHC QGSJetII-04 and EPOS-LHC models. The quoted systematic uncertainties arise primarily from the experimental measurement, a significant part of which is due to the 14% systematic uncertainty in FD energy. In this study, the energy systematic is necessarily transferred to a systematic in muon number.

This mixing of systematics is largely avoided in another Auger study, this time with more vertical (0°–60°) hybrid showers with energies between 6×10^{18} and 1.6×10^{19} eV (Ref. [132]). Simulated showers were generated using the EPOS-LHC and QGSJetII-04 hadronic models for pure protons, and for mass mixtures consistent with the Auger measurement for each model. Then for every one of the 411 real showers, the simulation library for a given model and mass option was searched for the best match to the real longitudinal profile as measured by the FD. The lateral distribution function of that simulated shower was then compared with that measured by the SD. On average, the simulations underestimated the signal $S(1000)$ for both models and both compositions, and the deficit was *not* constant with zenith angle. It is this zenith-angle dependence that reduces the degeneracy between a systematic shift in energy or muon content, since the FD is sensitive mainly to the electromagnetic component, and the SD is sensitive to both EM and muonic components, the mixture of which changes with zenith angle. The analysis results in rescale factors $R_{\rm had}$ for the muon content and R_E for the energy scale, for each model/composition combination. The data and the simulation can be brought into agreement with the application of $R_{\rm had}$ and/or R_E to the simulation. The results were that, for the mass mixture, the energy rescale factor was consistent with unity for both hadronic models: $R_E = 1.00 \pm 0.10$ for EPOS-LHC and $R_E = 1.00 \pm 0.14$ for QGSJetII-04, where the error is the statistical and systematic uncertainties added in quadrature. However, the magnitude of the rescale factors necessary for the simulated muon numbers to match the experiment were $R_{\rm had} = 1.33 \pm 0.16$ for EPOS-LHC and $R_{\rm had} = 1.61 \pm 0.21$ for QGSJetII-04, both improvements in the significance of the model discrepancies compared with the inclined air shower study discussed above. Obviously, the hadronic rescale factors required for a pure-proton composition were even larger.

Recent preliminary results from the TA Collaboration indicate that the muon content of EAS at distances between 2 and 4 km from the core of the shower is substantially larger by factors of 2 to 3 (at the 3σ level) than predictions from any of the current hadronic models for both proton and iron primaries. The improved sensitivity to muons is provided by making very selective cuts that maximize the absorption of electrons by the atmosphere. Results indicate that the discrepancy increases with core distance, which may imply problems with our understanding of the early part of EAS development, since the muons at large core distances would originate there (Ref. [133]).

These examples show that there is sensitivity for testing hadronic models with the current observatories, taking advantage of hybrid measurements of air showers with surface and fluorescence detectors. We can expect even better sensitivity in the future using surface detectors that can separately measure muon and electromagnetic shower components, e.g., with the upgraded Auger Observatory (Ref. [47]).

3. Challenges

3.1. Composition

3.1.1. Using the $X_{\max}$ measurement

Linsley (Ref. [134]) first proposed a simple way to look for changes in the cosmic ray composition as a function of energy. This involves the so-called elongation rate, or mean $X_{\max}$, as a function of energy. In a simple superposition model, a pure single component composition will have $\langle X_{\max}\rangle$ depend logarithmically on E with a constant change per decade (the elongation rate). A change in the composition would create an energy-dependent change in this rate. For example, a change from a lighter to a heavier composition would produce a decrease in the rate of change of mean $X_{\max}$ with energy (a flatter or even negative elongation rate). As long as there are no rapid changes in hadronic interaction physics, this is true in a model-independent way. However, the elongation rate does not tell us what the composition actually is. For this, hadronic models must be used to simulate air showers, the response of the fluorescence detector must be folded in or dealt with using cuts, and the resultant absolute position of $\langle X_{\max}\rangle$ must be compared with data at a number of energies.

There are a number of problems with this approach. First, the absolute predicted value of $\langle X_{\max}\rangle$ is hadronic model dependent, with variations of 10–20 g cm^{-2} between extreme models at any given energy. Then, the actual $X_{\max}$ distribution is asymmetric and if there is a significant protonic component it will have a long tail extending to deep $X_{\max}$. Heavier nuclei will have less pronounced tails. The mean value, $\langle X_{\max}\rangle$, is sensitive to these tails, which can be affected by detector systematics. This is one possible source of bias that can produce a systematic difference between simulations and data. Studies indicate that all the various effects can produce a net residual systematic in the mean $X_{\max}$ as large as 10–20 g cm^{-2} for the TA experiment (Ref. [25]), and up to 10 g cm^{-2} for the Auger experiment (Ref. [27]). Unless care is taken, undersampling due to low statistics may also shift $\langle X_{\max}\rangle$. The second moment of the distribution, the RMS, is sensitive to both the tails and the width of the distribution and hence carries additional information. The RMS is less hadronic model dependent since the distribution width mostly depends on superposition. A change of RMS from 60 g cm^{-2} (characteristic of proton showers for essentially all hadronic models) to 30 g cm^{-2} as a function of energy is observed by the Auger Collaboration (Ref. [27]) in the energy range above 10^{18} eV and it can be considered evidence for a change in composition. The smaller RMS can be produced only by heavier nuclei such as CNO or Fe, again in an essentially model-independent way. However, the RMS measurement suffers some of the same systematic problems as the elongation

rate. Undersampling of the tail of a distribution, either due to low statistics or detector bias, can mimic a composition change. The Auger Collaboration has been able to address this in some detail because of its high statistics (Ref. [27]). The TA measurements at the highest energies still suffer from insufficient statistics to address this issue completely.

A puzzling issue that has emerged from this approach is that it is difficult to reconcile the $\langle X_{\rm max}\rangle$ with the RMS distributions. For example, in a simple 2-component p/Fe model, the RMS at the highest energies agrees well with a nearly pure Fe composition but the $\langle X_{\rm max}\rangle$ requires a much lighter mix. Reproducing this is a struggle even with a 4-component composition.

For all these reasons, comparison of the full $X_{\rm max}$ distribution between data and Monte Carlo (MC) simulations seems the best approach. In principle it provides the maximum information. However, a straightforward statistical comparison of data and simulations is made impractical because of the presence of significant systematic uncertainties both in the data (overall $X_{\rm max}$ position) and the hadronic model.

There are 2 approaches to deal with the problem of determining composition. The TA and HiRes Collaborations apply loose cuts to data (sufficient to ensure good resolution) and carefully simulate p, He, N, and Fe air showers based on a variety of hadronic models. Whatever distortions in the $X_{\rm max}$ distribution are generated by the detection method and reconstruction should then be evident in the reconstructed simulated data. The Auger Collaboration instead applies much tighter fiducial volume cuts that minimize any detector and reconstruction bias. The resulting data can then be directly compared to the "thrown" simulations. Direct comparison of the data from these 2 approaches can be problematic since the detector distortions will be different, though the biases in the most recent TA hybrid analysis are much smaller than for previous results.

Recently, the Auger and TA groups have developed a method to improve comparison of $X_{\rm max}$ distributions (Ref. [107]). The Auger group fits their cut and unbiased data to a simulated composition mixture as a function of energy. The resultant composition fractions are then used by the TA group to generate "thrown" simulations. These are then processed through the TA reconstruction process and compared to the data. Preliminary results show agreement within the systematic uncertainty for the overall elongation rate. This approach is, in principle, independent of the hadronic model used, since this is used only as a method to port one data set into another experiment's acceptance.

But how does one deal with systematic uncertainties in these comparisons? What is needed is a comparison method that allows for a sliding $X_{\rm max}$ scale (to take account of overall systematics) while preserving the shape of the distribution. The TA group has proposed such a method (Ref. [101]) that first removes the energy dependence of the distributions and allows an $X_{\rm max}$ shift for the data that is determined by the best overall $X_{\rm max}$ profile fit. One can then compare the distribution shape goodness of fit to the required sliding $X_{\rm max}$ scale factor to see how well any given composition assumption does when compared to the data. For example, if the scale factor shift required is well beyond the estimated systematic uncertainties and there is a poor profile shape fit, then that hypothesis can be discarded.

Another approach, used by Auger (Ref. [30]), is to directly compare a multicomponent mix of simulated showers with the data. This is done for a variety of hadronic models. This approach uses p, He, N, and Fe as markers for the actual cosmic ray composition. The QGSJetII-04, Sibyll 2.1, and EPOS-LHC hadronic models are used. The individual components have separate weights that vary as a function of energy and the experimental systematics are folded in to the degree that they are known. The results change as one shifts hadronic model assumptions; while an overall trend of moving from p to He in the energy range from $10^{18.3}$–$10^{18.8}$ eV is shared by all 3 models, only EPOS-LHC gives a

nearly constant and large fraction of N (∼40%) across the full energy span, while the other 2 models are consistent with an almost zero N fraction. Above $10^{18.8}$ eV, dominant components are He and N, but their proportions are very much model dependent; EPOS-LHC favors N while the other 2 models strongly support He. These differences make an astrophysical interpretation challenging as they are most likely due to model inadequacies. While the details are not clear, the required proton fraction decreases above 3×10^{18} eV and there is no requirement for any significant iron fraction.

The lack of consistency is not surprising given that even for a single hadronic model, HiRes publications (Ref. [135]) have noted that introducing more than 2 components into a fit to an $X_{\rm max}$ distribution does not lead to an easily interpretable result, as various combinations can give equally good fits. In the case of Auger, the best fits are produced with more than 2 components, but the uniqueness of the interpretation remains problematic.

Any particular approach to reconstruction shower profiles has hidden systematics that are intrinsic to the chosen approach and the particular software implementation. This systematic uncertainty is separate from detector or atmospheric systematics. Two different, error-free, reconstruction programs that use different approaches (different binning, least-squares fitting routines, tabular vs functional corrections, etc.) will produce slightly different results. The TA group has explored this "intrinsic" systematic by comparing completely independent and otherwise well-vetted hybrid reconstruction programs, as well as by comparing results from stereo data. They find that it is very difficult to make the $X_{\rm max}$ distributions (for the same data or simulations) agree to better than 5–10 g cm^{-2} (W. Hanlon, personal communication; Ref. [27]). This seems to be an irreducible systematic uncertainty.

A particular complication in the study of cosmic ray composition is the fact that any nucleus heavier than a proton will eventually fragment to a lighter nucleus as it travels from its source to the Earth. This fragmentation is due to the interaction of the nucleus with both the relic 2.7 K black body photons and the IR radiation fields produced by stellar radiation (Refs. [94,136–138]). As a result, even a pure single nucleus composition heavier than a proton at the source should appear as a mixed composition. A pure proton primary composition will arrive intact, but observation of a proton component cannot rule out that part of this component is due to heavier nuclei. On the other hand, observation of an iron component uniquely indicates the existence of a primary iron at the source, since stellar nucleo-synthesis does not provide any significant concentration of nuclei above iron. Propagation models show that He, CNO, and Fe have different spallation probabilities as a function of energy (Refs. [139,140]). This is particularly evident above 3×10^{19} eV where the He mean free path is on the order of 10 Mpc, compared to ∼100 Mpc for N (Ref. [94]). An He-dominated flux above 3×10^{19} eV makes sense only if sources are very close. The lack of anisotropy makes any such assertion implausible. Indeed, propagation calculations indicate that, integrated over the large-scale structure, the mean A of nuclei originating as He is essentially 1 (Ref. [140]). If the observed He is the result of fragmentation of heavier nuclei, then a proper proportion of these heavy nuclei, whose mean free paths are much longer, must also be seen in the composition distribution. Incorporating the observed cosmic ray nuclear abundances found with a particular hadronic model directly with propagation effect weights in a more direct fashion than is currently done could be very helpful. In some cases, this may rule out an otherwise well-fitting model as leading to astrophysically implausible scenarios.

3.1.2. Implications of the lack of iron in UHECR

While the systematic uncertainties in $X_{\rm max}$ determination and comparison to simulated compositions are still too large to make strong statements about the relative abundance of elements in the cosmic

ray flux at Earth or at their origin, we have learned that there is very little iron in the flux above 10^{18} eV. Given existing systematic uncertainties, it is safe to say that any direct or secondary heavy nuclei from Fe to Si are absent from the spectrum. We know this absence with better precision than we know what elements are present in the flux. What does this imply about the sources and acceleration mechanisms of UHECR? UHE primary iron can easily reach the Earth from as far away as 100 Mpc and its spallated by-products down to Si from much further distances. Are magnetic field effects strong enough to substantially increase the effective path length? Is there a deficit of iron in the cosmic material feeding the accelerator? There is astronomical evidence that iron attaches itself to dust particles and hence appears to be somewhat depleted in its free form; see, e.g., Refs. [141–143]. However, why the iron-rich dust particles cannot be swept from an accretion disk into the accelerator beam, decomposed to their atomic constituents, and provide the original iron abundance is not clear. With a charge 26 times that of a proton, iron will be accelerated quite efficiently at the highest energies. If iron is indeed accelerated at the source then its absence must require photon fluxes at the source that essentially eliminate it from the cosmic ray flux. The absence of heavy elements in the cosmic ray spectrum may thus be an important constraint and a clue to cosmic ray origins.

3.1.3. FD/SD energy mismatch, muon excess

Much of the progress in establishing the structures in the cosmic ray spectrum come from the reliable energy scale provided by air fluorescence. With an ∼15% FD energy resolution and similar systematics, calibrating the SD energy scale to simultaneously observed FD events has made the SD spectrum energy largely hadronic model independent (Ref. [144]). For the TA case, the energy scale adjustment that needs to be made between the FD and SD is on the order of 25%–30% if one uses QGSJetII-03 proton simulations for the SD energy. The measured particle densities produce a lateral distribution that, were it analyzed based on hadronic model simulations of air showers, would generate too high an energy by this amount. In other words, there are too many charged particles at ground level for a shower with an energy as determined by the FDs. Because Auger water-Cherenkov detectors are quite sensitive to muons, this mismatch has been attributed to an excess of muons in the data compared with expectation. In the case of TA's plastic scintillation detectors, electrons and muons have similar detector response and the mismatch can be only partly attributed to a muon excess. Studies are proceeding to investigate whether scintillation detectors at large distances from the core, which should have mainly muon-initiated signals, are consistent with the Auger results (Ref. [133]). In any case, it is clear that the hadronic models that are used to simulate showers are not adequate. Until this issue is resolved it is difficult to use muon density to measure cosmic ray composition precisely, though trends can certainly be established (see below).

3.1.4. Other techniques

(a) Radio The fluorescence technique revolutionized the study of UHECR physics because it made possible a largely calorimetric determination of the energy scale and a relatively direct measure of composition using the $X_{\max}$ of the showers. It requires clear moonless nights, which restricts its on-time to 10%–15% of the SD operation times. Recently, a great deal of work has been done in investigating the possibility of using radio emission from EAS in much the same way as one now uses fluorescence (Ref. [145]). Radio can, in principle, determine the shower energy and $X_{\max}$ and would have the advantage of ∼100% on-time. A number of radio arrays have now been operating either stand-alone or in conjunction with surface and air fluorescence detectors (Refs. [146–148]). Because there are several mechanisms in the air shower development that can generate radio waves, the

detailed simulation has taken some time to develop but now seems sufficiently advanced. Meaningful comparisons with real data have been done and good agreement is now evident between simulations and radio and SD measurements (Ref. [149]). These studies have been largely limited to energies less than 10^{18} eV however, and in this energy regime it appears that an array of radio antennas with spacings not dissimilar to SD spacings are required for good energy and $X_{\rm max}$ resolution. If similar spacings are required for $>10^{18}$ eV energies, the costs associated with instrumenting $>1000\,{\rm km}^2$ arrays become significant. Until more complete optimization and cost/benefit analyses for the UHECR regime are done, it is not clear that this technique will supplant fluorescence and particle SD arrays. In any case, significant physics from the low-energy arrays is required before this new technique can be considered fully vetted.

(b) $X_{\rm max}$—SD signal correlations Recently, an approach to studying composition has been proposed using the correlation between $X_{\rm max}$ and the SD signal (Ref. [111]). This is based on the very old idea that if iron and proton showers have different $X_{\rm max}$ distributions and different N_μ distributions, then superposing their $X_{\rm max}$–N_μ scatterplots will lead to a negative correlation even though the pure distributions have a positive correlation. Since this is generally true of any hadronic model, the claim of this approach is that this is more model independent than either a pure $X_{\rm max}$ or pure N_μ analysis. However, since neither Auger or TA actually measure N_μ (except at large zenith angles in the case of Auger) the searched-for correlation is with $S(1000)$ or $S(800)$. The recent work on this by Auger (Ref. [111]) shows that in the $10^{18.5}$–$10^{19.0}$ eV energy region, the correlation is inconsistent with a pure composition. A preliminary study by the TA Collaboration on the other hand shows no inconsistency with the assumption of a protonic composition (J. P. Lindquist, personal communication). However, in the case of TA, the method is not nearly as sensitive as the $X_{\rm max}$ method. This may be because the muon content in TA is not as large a component of the SD signal as for Auger. Since the method is de facto dependent on detector muon sensitivity, it must also be to some extent model dependent, although the Auger study checks this with 2 independent models. Studying the applicability of this method in the lower-energy region (10^{18}–$10^{18.5}$ eV) would be of interest since there the composition is likely to be more pure, given both the Auger and TA $X_{\rm max}$ data.

3.2. Energy

One of the most significant results coming from Auger and TA is the overall agreement in the shape of the UHECR spectrum. At first glance, both spectra show a clear ankle structure and a cutoff, although the precise energies for these structures differ. However, a shift of either experiment's energy scale by 10%–15% brings the ankle structure into excellent agreement (Ref. [80]). Since such a shift is within the systematic uncertainties of either experiment, it would seem that there are no significant north–south differences here. A closer look at the ratio of the 2 spectra shows, however, that the location and shape of the cutoff seems different at the $\sim 3\sigma$ level (Refs. [38,150]). The Auger/TA combined working groups have looked at this difference and, so far, have found no reason to believe it is a result of systematic uncertainties in energy. If this is truly a difference in the flux of northern and southern sources at the highest energies, there should be an overall declination dependence. Preliminary evidence from TA indicates that the TA spectrum becomes much more like the Auger spectrum near the cutoff if a declination cut of $<25°$ is made (D. Ivanov, personal communication). The difference (a higher energy cutoff for TA) must then come from higher declinations, which also contain the "hotspot" that may be a signature for a relatively nearby source. While this is suggestive,

much more work needs to be done to demonstrate that this cannot be a systematic effect either in energy or aperture estimation.

3.2.1. Energy scale shift systematics

As indicated above, the ankle structure that is seen with high statistics in both TA and Auger data can be used to estimate the difference in energy scale of the 2 experiments. While the result is within systematic uncertainty estimates, it is important to understand the nature of the energy shift as well as possible. Given the current precise nature of shower reconstruction, differences in energy can most likely be attributed to systematic uncertainties in optical properties (mirror reflectivity, light collection efficiency, etc.), phototube gain calibration, atmospheric transmission, and air fluorescence efficiency. All but the last are by their nature detector dependent and we must rely on the diligence of the experimenters in estimating how well they know these parameters.

The air fluorescence efficiency is in principle a common factor, though it depends on humidity and temperature corrections that may be somewhat different in the 2 locations. For reasons of keeping a historically consistent energy scale, the HiRes and TA groups have used the original Kakimoto et al. overall yield measurement (Ref. [65]) while a subset of Auger Collaborators have launched a series of special experiments to measure the fluorescence yield more precisely with AIRFLY (Refs. [67,151]). The HiRes group also performed a series of measurements using an electron beam at SLAC (FLASH (Refs. [152–154])) but only the relative spectral line strength measurement has so far been incorporated in the TA analysis. The TA experiment also includes a 40 MeV electron linac whose vertical beam is seen in the field of view of one of the fluorescence detectors. Work on understanding the results of this in situ measurement is proceeding (Ref. [63]). All contemporary measurements of the absolute value of air fluorescence rely on a fixed-energy electron or proton beam that deposits energy in a small pressure-controlled chamber. Significant corrections for deposited energy escaping the chamber (in the form of delta and gamma rays) must be made. The MACFLY (Ref. [155]) and thick target FLASH experiments generated a shower in an air-equivalent material and observed the fluorescence as a function of the absorber. Neither of these experiments was able to produce an absolute value for the fluorescence efficiency with sufficiently small uncertainties to compete with the thin target experiments, though they did show that the relative longitudinal development of showers is well tracked by the resultant air fluorescence. Recently, a new experiment at SLAC called sFLASH (P. Sokolsky, personal communication) is attempting a $<10\%$ total systematic uncertainty measurement of air fluorescence from a ~ 10 GeV electron shower developing at sea level and observed near shower maximum. If successful, this will be a valuable cross-check on the thin target results. What is lacking is a common air fluorescence result that is used for both TA and Auger analysis. It is to be hoped that such a convergence can occur in the near future.

3.3. Anisotropy

Large-scale anisotropy can be searched for using a multipole expansion. This is, however, tricky to do without bias unless one has full coverage over the celestial sphere. It is thus very advantageous to combine TA and Auger arrival direction data. There are several challenges to using this data set however. Because of the energy scale difference one cannot simply apply the same energy cut for both data samples. There are also potential systematic differences in determining the detector apertures of the 2 detectors. The Auger/TA anisotropy working group has developed an approach that uses the overlapping declination band for the 2 detectors (Ref. [92]). The fluxes in this band are normalized and this normalization is carried over to the total data set. The assumption here is that the spectrum

has no significant declination dependence in the overlap band. The resultant distributions have yet to show any statistically significant dipole or quadrupole moments, though Auger itself observes a significant dipole enhancement (Ref. [87]). A better understanding of the energy-scale shift between the 2 experiments, and strategies to deal with it, could provide a simpler method of combining data without additional assumptions.

3.4. TA hotspot

With the fading of the Auger association of UHECR with AGN (Refs. [95,156]), the community's hope for finding clear associations of cosmic ray arrival directions with astrophysical sources has received a lift with the possible observation (at the 3.4σ level) of a concentration of cosmic rays with energies above 5.7×10^{19} eV in the northern sky by the TA experiment (Ref. [88]). This "hotspot" of 20° radius is observed near Ursa Major, about 10° off the supergalactic plane. If this intermediate-scale anisotropy is confirmed with more statistics, its location raises interesting questions, since none of the previously assumed cosmic ray sources (e.g., the Virgo cluster) are in the immediate vicinity. If the sources are actually in the adjacent portion of the supergalactic plane, then there must be a magnetic field effect shifting the flux to the observed location. A suggestion has been proposed that there is a magnetic flux tube produced by a filament of galaxies connecting the hotspot to sources such as M87 (D. Ryu, personal communication). Another possibility is M82, which is sufficiently close to account for the hotspot using currently estimated magnetic fields. Tidal disruption events creating one or more flashes of extremely high-energy protons or nuclei have been proposed for the acceleration mechanism (Refs. [157,158]). If this hotspot strengthens in significance it will pose a challenge to our understanding of sources and magnetic field configurations.

If medium- or small-scale anisotropy is finally observed, the next major challenge is to correlate our composition-related information with arrival direction information. Hybrid FD plus SD data would be the most convincing, but requires the most running time for any given source. If the muon content of showers can be better understood and correlated with composition, this could give the most sensitive composition-dependent anisotropy measurement. It is unfortunate that the currently most likely source (TA hotspot) and the major Auger upgrade of their SDs to better detect muons correspond to disconnected parts of the sky. If the hotspot is confirmed, and the muon content becomes better understood, coming to grips with this issue will be one of the major challenges for this community.

4. Future observations

4.1. Extension and upgrade of ground observatories

Above the "knee" at around 10^{16} eV, the cosmic ray energy spectrum and $X_{\rm max}$ measurement demonstrate rich features, and around 10^{19} eV and above, various anisotropies seem to show up in the energy spectrum and flux. Where statistics are adequate, no obvious inconsistency is found in the $X_{\rm max}$ measurements in the northern and southern hemispheres above 10^{18} eV, but their interpretation allows a range of composition mixes and energy dependencies due to statistical and systematic limitations. It is important for Auger and TA to cover the entire sky and the whole energy region together, in order to bring these indications to a consistent set of observational facts. It will become the basis of locating the galactic to extragalactic transition energy of cosmic rays sources, and of building a viable astrophysical model to explain the production and propagation of UHECR. Continuing to challenge this physics, TA and Auger are both planning to start the operation of extended and upgraded detectors around 2018–19.

In the northern hemisphere, TA×4, the extension of TA (Refs. [159,160]), is in preparation. It will extend the aperture of the SD by a factor of 4 by 2018. Leaving a part of the SD intact with 1.2 km spacing, an extended part will have a 2.08 km spacing, together covering a 3000 km^2 ground area. Adding 2 more FD stations, the hybrid coverage will be tripled. The trigger efficiency of the extended SD will be larger than 95% for $E \gtrsim 10^{19.8}$ eV. Resolutions will be slightly compromised to become ∼25% for energy and 2.2° for the arrival direction. In 3 years of running, over 2018–2021, the number of SD events above 57 EeV (=$10^{19.76}$ eV) will be quadrupled to become 300, of which ∼80 would be in the hotspot region, assuming the flux of Ref. [88]. The measurement range of $\langle X_{\rm max} \rangle$ using hybrid events will be extended to $\sim 10^{19.6}$ eV from the present $10^{19.4}$ eV (Ref. [101]). The SD design of the TA×4 was re-optimized to use a much shorter length of wavelength shifting fibers (1/3 of the length in the TA/SD) while keeping the same number of photo-electrons collected by the PMT for a minimum ionizing particle. The quantum efficiency and the linear range of the PMT is nearly doubled.

In the southern hemisphere, the Auger Observatory plans to upgrade the detector to AugerPrime by 2018 (Ref. [47]). All the ∼1600 stations will be equipped with a 3.8 m^2 plastic scintillator on top and the wave-form sampling electronics will become 3 times faster (to 120 MHz). An integrated analysis of water-Cherenkov and scintillator signals will enable an isolation of muonic and electromagnetic (EM) energy deposits, and enable the counting of the number of muons hitting the SD. New methods are being developed to estimate $X_{\rm max}$ from SD measurements alone, taking advantage of so-called shower universality (Ref. [161]). The search for small-scale anisotropy and source correlation is expected to improve significantly by selecting SD events with high likelihood of being protons or light nuclei. The muon identification is double-checked for a portion of SD events using an array of scintillators buried 2.3 m underground. The duty cycle of FD operation is expected to become 1.5 times larger by tolerating data collection with a higher night sky background. The mixed composition result (Ref. [30]) will be further checked with measurements from the FD together with the enhanced SD with its own measurements of $X_{\rm max}$ and muon content. AugerPrime and TA×4 together will have all-sky coverage with a total of 6000 km^2 of surface area: one at 39° north and the other at 35° south. The overlapping region at low declinations (−16° to +45°) will be important in understanding the relative exposures and to examine systematics of the detectors and data analyses.

Air shower detectors operating in the last decade have reported a series of Earth-science related findings: TA's SD recorded bursts of particle showers associated with lightning (Refs. [162,163]), the development of distant atmospheric "elves" was recorded by Auger (Refs. [164,165]), and the LOPES radio signal from air showers was modulated by thunder-clouds (Ref. [166]), etc. UHECR observatories may become an interesting research tool for Earth and atmospheric sciences in the next decade.

4.2. Development of radio detection

Understanding the mechanism of air showers generating radio signals in the sub-100 MHz range has advanced greatly in the last decade (see Refs. [145,167] for reviews). Newly developed simulation codes tell us that the radio signal comes from 2 types of time-varying, fast-moving effective charges generated in the air shower; one is the lateral movement of shower $e^{\pm}$ under the geomagnetic field and the other is the longitudinal movement of net charge in the shower front (the Askaryan effect). Both signals scale with the square of the electromagnetic energy ($\propto E^2$). The signal is sharply forward peaked in the direction of air shower development and stands well above the galactic radio noise for

energies exceeding 10^{16} eV. The radio telescope LOFAR, operating in cosmic ray detection mode, realized a very fine radio sampling of air showers, and succeeded in observing air showers of energy 10^{17}–$10^{17.5}$ eV with a typical $X_{\max}$ reconstruction uncertainty of 17 g cm^{-2} (Ref. [146]).

The AERA radio array with varied antenna spacing has been deployed at the Auger site for testing the detection of the highest-energy showers (Refs. [147,148]). The results demonstrate that a dense deployment of antennae is required for the effective detection of UHECR that have a footprint of several hundred meters in diameter. Even though the elements of the RD (radio detector) may be relatively simple and inexpensive, the total cost of deploying and operating a large area detector would become prohibitive. One practical application for UHECR is for the measurement of very inclined air showers with $\theta > 70°$, which has an extended oval footprint larger than 10 km^2. Such RDs deployed together with the SD may also be used for the calibration of SD energy, making use of the fact that the radio signal originates predominantly from the EM component of the shower, and that it has a negligible attenuation in the atmosphere. Note that this is the kinematic region where precise measurements by standard SD techniques, using a water-Cherenkov station or a scintillator, have large uncertainties, and redundant information is useful. The radio detector is also expected to have a high duty factor of ∼95%.

Another direction of progress foreseen for using radio signals from EAS is the detection of high-energy neutrino-induced showers in the Antarctic ice via the Askaryan effect. Pioneering work searching for such short, gigahertz-polarized radio signals from the horizon in Antarctica began with the ANITA balloon experiment in 2006 (Ref. [168]). Its fourth flight was launched in December 2016. The ARA and ARIANNA experiments were recently proposed and extensive RD is underway to detect the Askaryan signal from cosmogenic neutrinos near or on the surface of the Antarctic ice (Refs. [168,169]).

Searches for gigahertz-"molecular Bremsstrahlung" radio emission from particle showers in the atmosphere (Ref. [171]) have so far not been successful (Refs. [172,173]). Also, a limit has been set by the TARA experiment at the TA site for detecting the modulation of 54.1 MHz carrier radio waves by the ionized column generated by a UHECR shower in the atmosphere (Ref. [174]).

4.3. Observations from space

The EUSO International Collaboration was formed in 2000 to install a wide field of view (FoV) telescope at the International Space Station (ISS) to look down on the Earth's atmosphere and search for air fluorescence flashes from UHECR (Ref. [175]). The JEM-EUSO detector employs a Fresnel lens telescope with a diameter of 2.4 m and a 60° FoV, covering a ground area of 200 km radius from an altitude of 400 km (Ref. [176]). The effective ground coverage with the expected duty factor of 20% is 28 000 km^2, or approximately 5 times that of AugerPrime and TA×4 combined. A tilted mode of observation would increase the acceptance by a factor of 3 or more at the cost of reduced resolution and higher detection threshold. The ISS inclination angle of 51.6° allows a uniform survey of the Earth's atmosphere in the northern and southern hemispheres with nearly the same acceptance and event geometry. The observations from high altitude and the limited optical entrance pupil of the Fresnel lens will however limit the JEM-EUSO detection threshold to be $\sim 10^{19.5}$ eV, and the $X_{\max}$ resolution is foreseen to be larger than 60 g cm^{-2} in the nadir mode (Ref. [177]), making the differentiation of nuclear composition difficult.

The mission schedule of JEM-EUSO is yet to be determined, but an extensive series of tests of the prototype instruments is being performed (Ref. [178]). Major efforts include the balloon-borne EUSO-SPB test (2017), and deployments of mini-EUSO (2017) and K-EUSO (2020) at the ISS.

The K-EUSO experiment will have a segmented Fresnel mirror 3.4 m in diameter, and its effective coverage of the ground will be 6200 km^2 above $10^{19.5}$ eV, about equivalent to AugerPrime and TA×4 combined. An exploring Russian satellite experiment, TUS, with similar optics was launched in 2016 and is being commissioned (Ref. [179]). The uniform all-sky coverage of K-EUSO will be very important in understanding the nature of the north–south anisotropy, or the inconsistency of the flux, being seen by TA and Auger.

4.4. A future ground observatory

Given that observations by the extended ground detectors will proceed well into the next decade, and that exploratory space projects will start giving a large acceptance coverage of the entire sky, what are the new and/or remaining challenges for future ground observatories (FGO) of ultra-high energy cosmic rays? In this section, we take "Auger×10" as a hypothetical example of an FGO, and discuss how the FGO might look, and how research might proceed with the FGO.

FGO We assume "Auger×10" is a symmetric set of northern and southern observatories, each with 30 000 km^2 ground area, covered in whole by hybrid arrays of FDs and SDs. An array of radio detectors (RDs) may be overlaid on the SD to enhance the energy and possibly the $X_{\rm max}$ determination for inclined events, improving the quality of all-sky coverage. We assume the SD is equipped with a particle identification function for a fraction of shower particles, and that this is to be used for the likelihood tagging of the primary composition. Approximately 10% of events are SD–FD hybrid, which offers a direct means of composition determination via $X_{\rm max}$.

Composition at the cutoff Such an FGO will collect approximately 10 000 SD events above $E_{1/2}$ ($10^{19.8}$ eV for TA) or above E_s ($10^{19.6}$ eV for Auger) in 10 years of operation, of which about 1000 events will be SD–FD hybrid. Protons and iron are the natural nuclear species to compose a cutoff structure, due to their expected abundance at the acceleration site and their comparative stability in the subsequent propagation in the nearby (∼100 Mpc) universe. Indeed propagation calculations indicate that cosmic rays above energies of $10^{19.5}$ eV will have a simplified, approximately bimodal arrival composition, even if they are produced in equal proportions from protons to iron at the source. Intermediate mass nuclei will appear mostly as proton and He spallation by-products. Thanks to the high statistics, the improved $X_{\rm max}$ resolution and the additional $\rm N_\mu$ information of the FGO hybrid events, we expect that contributions of protons and iron will clearly stand out in an $X_{\rm max}$–N_μ scatterplot. Protons or iron at the cutoff will be a straightforward confirmation of the existence of the corresponding astrophysical mechanism that creates the strong suppression, either the GZK or the acceleration limit scenarios.

If protons and iron were both identified in the hybrid sample it would allow the measured estimators of composition, $X_{\rm max}$ and N_μ, and their predictions by the simulation code, to be "calibrated" by the observation. Even when contributions of He, CNO, and heavier nuclei are significant (and the isolation of protons and iron is not obvious), we still expect proton and iron contributions, because the existence of He results in (spallation) protons, and the existence of CNO calls for the parent Fe of the spallation (see Sects. 3.1.1 and 3.1.2 for a discussion). The statistics of the FGO hybrid sample, 1000 events above $E_{1/2}$ or E_s, would allow a reasonable "calibration" or cross-check to be performed for compositions in the range of protons (Z=1) to iron (Z=26).

Composition-dependent anisotropy and energy spectrum The SD and RD events of the FGO are tagged with a likely primary mass derived from the $X_{\max}$ and N_μ analysis, both of which are being calibrated using hybrid events. The statistics of these events, 10 000 or more in total above the flux suppression, is enough to allow the flux, energy spectrum, and composition of UHECR to be separately determined in ∼100 different sections of the sky. Their correlations, such as the "proton/iron sky above a certain energy" and the "energy spectrum of proton/He/CNO/iron in particular sections of the sky", can be plotted from a single unified event sample. This will be very effective in establishing astrophysical models to explain the observed features of UHECR. Searches for autocorrelation and association with astrophysical sources, as well as the multimessenger analysis, will be effectively made using the tag of primary composition.

As a result, we can continue investigating the nature of galactic and extragalactic magnetic fields, background photons in the universe, cosmological development of UHECR sources, special relativity with exceptionally high Lorentz factors, and other subjects in astro-particle physics.

Cosmogenic ν's and γ's The search for UHE neutrinos and gamma rays by the FGO will be limited only by statistics, using the primary composition tagging of the FGO/SD. The sensitivity to cosmological neutrinos and gamma rays will allow us to enter the region of possible detection, or of placing significant limits on standard predictions (see Sect. 2.7).

UHE interactions Our understanding of ultra-high energy air showers is incomplete: the data from present detectors indicate that the number of shower particles in the off-core region is larger than the simulation program predicts, or that the simulated air shower is "slimmer" than the real one (see Sect. 2.8.2). Using a large collecting area and high sensitivity for penetrating particles, this is most clearly demonstrated for muons detected in the Auger water-Cherenkov stations. The difference between the data and the simulation remains after the ambiguities from energy determination and primary composition are removed, and updated hadronic interaction models with the LHC data are used (Ref. [132]). Using composition-tagged SD events of the FGO, the lateral distribution of muons and electrons in the off-core region, and its relation to the primary energy and composition will be studied. The measurements are to be compared with a variety of model predictions with the highest-energy LHC data, including taking into account nucleus–nucleus collisions.

In the case where a certain region of the sky is identified as protonic without significant contributions of heavier components, the ankle and the cutoff features in this region could possibly be attributed to the pair-production on the CMB and the GZK effect, and the corresponding energies can be used for calibrating the energy scale of the incoming protons. While it is possible that there may still be a contribution from galactic protons, this can be checked by examining the ratio of the ankle to GZK energies and the Berezinsky modification factor (Ref. [180]) as a function of light/heavy anisotropy. In any case, the possible anisotropies of these ratios would be of great importance in constraining cosmic ray origin and propagation models. Given that these features can be associated with pair production and the GZK cutoff, then the difference between the expected primary energy and the measured calorimetric energy by the FD or RD is to be accounted for by the "invisible energy" carried underground by the very-high energy muons and neutrinos in the shower core region. In this way, we expect ultra-high energy air showers will remain as a source of observational information for the study of the nature of hadronic and nuclear interactions beyond collider energies.

FD Measuring the energy and composition of UHECR will remain a basic mission of the FGO. The FGO/FD does this by covering the entire acceptance, but with a limited duty cycle of ∼10%. The FGO/RD would cover a limited acceptance at large θ but with a duty cycle higher than 90%, and its eventual contribution may become significant. When working in hybrid mode with the SD, some of the FD information is redundant. This leads to the FAST concept of deploying an array of compact, wide-angle, and essentially single-pixel FD telescopes that record the time development of air fluorescence in multiple stations (Ref. [181]). The reconstruction of the shower core location and arrival direction may be achieved mainly by using the SD information, and the time variation of the FAST signal is then converted into the longitudinal development of the shower. The FAST detector would work exclusively for supplying the calorimetric energy and $X_{\rm max}$ information of the event. Optimization studies have been performed with the goal of obtaining good resolution with limited photon statistics. Controlling the effect of background photons on-line for the trigger and data acquisition remains a technical challenge. A small FD telescope with a similar concept has been tested by the CRAFFT team (Ref. [182]). The current design of FAST assumes FD stations with 360° azimuthal coverage on a rectangular grid of 20 km separation. A total of 75×2 FD stations will be necessary to cover the entire FGO acceptance in the northern and southern hemispheres.

SD The FGO/SD is expected to have a good particle identification capability for shower particles. The isolation of muons will be of particular importance, and various types of detectors have been tested during the design study of AugerPrime using the existing water-Cherenkov station as a bulk muon counter and absorber of the EM component. Here we remind the reader of another example, the "lead burger": a sandwich of segmented scintillator and lead absorber, tested in the AGASA array as a candidate for the original Auger SD detector (Refs. [183,184]). Advances in photo-detectors and electronics may now allow a significantly finer detector segmentation and fast wave-form sampling, strengthening the multihit capability of the lead burger (Refs. [185–187]). The dE/dX measurement and coarse tracking of individual particles may also be incorporated. Besides muon identification, detection of spallation neutrons may be possible for tagging the nuclear composition and identifying primary gamma rays. TA and Auger are ideal testing grounds for developing the FGO/SD and for optimizing its performance. Taking the 2.1 km grid spacing of TA×4 as an example, 6900×2 SD units will be necessary to fill the FGO acceptance.

Electronics and network The FGO electronics may follow the base design of Auger and TA with FADC sampling of wave forms, multilevel digital triggers, and wireless communication networks. For the FGO/SD, the number of readout channels must be significantly increased for the segmented detector and for the integration of FGO/RD, and faster digitization is required for better timing measurement. The biggest challenge would be that all these performance upgrades need to be realized with a limited power budget due to local electricity generation and storage. Taking advantage of the low duty cycle of SD digitization electronics, clever methods could be invented to save electric power consumption.

Reliability and fault tolerance are required for the stable operation of many FGO/SDs distributed over a large ground area. With a steady increase of locally available computing and data storage capacities, real-time requirements for trigger generation and data acquisition may be loosened, and greater autonomy may be allowed for the operation of individual SDs. This in turn reduces the network load of communications between SDs, and increases the overall system reliability. It may also allow for the whole communication system of the FGO to reside on a standard communication

network. This will be advantageous in terms of construction cost, long-term operation, and for taking advantage of progress in communication technologies and updates in the DAQ system. Implementing a prompt coincidence trigger formed over several clustered SDs, assuming it is required, may be a technical challenge in building such an autonomous DAQ system.

For the FGO/FD array, the load on digitization electronics will decrease compared with the current many-channel system, but triggering on a limited number of sensor pixels will be itself a challenging task. A clever time coincidence method between the neighboring SDs and FDs, or the introduction of an external trigger via the network, may be a resolution to this problem. Reliable remote operation of the telescopes, monitoring and calibration devices via the wireless network is the key to the success of achieving good operational performance of the FGO.

Collaboration The construction and operation of the FGO will be a challenge for technology, management, and resources. It may be accomplished only through a collaboration of people with zeal, having excellent expertise and experience. Some of the features of the FGO detector, electronics, and communication system have already been discussed in the proposals for northern Auger and AugerPrime (Refs. [46,47]). The physics issues, and an experiment of similar sensitivity to the FGO known as "TA2", have been discussed in physics community meetings in Japan.

5. Conclusion

The era of very large observatories has produced many new and important insights into the properties of the ultra-high energy cosmic ray flux. This has been achieved with well-designed detectors and very large collecting areas, with important design input from previous generations of experiments. An important feature of both Auger and TA is the hybrid nature of the observations. Apart from providing calorimetric energy measurements, a hybrid observatory offers a multitude of cross-checks that have improved the measurements and reduced the systematic uncertainties.

The UHECR energy spectrum is now measured with high statistics, resulting from a combined Auger/TA exposure of over 60 000 km^2 sr yr at the highest energies. The spectrum now reveals several features, including an unambiguous suppression beyond 4×10^{19} eV. A dipole anisotropy has been observed for the first time at ultra-high energies, and there is great interest in the possible northern hemisphere "hotspot" over a 20° radius area of sky that will be monitored by TA×4 for an increase in significance in coming years.

Small-scale anisotropies and associations of cosmic ray arrival directions with astronomical catalogs have not been convincingly observed. It is probably fair to say that this lack of success was not expected. This may be related to an apparent increase in the cosmic ray mass and charge above the ankle of the energy spectrum. While not currently embraced by the entire community, a heavier flux would help to explain the lack of small-scale anisotropy. On the other hand, if the northern hemisphere "hotspot" persists, its appearance may be related to mass composition differences between the north and the south. The difference between the flux suppression energies between Auger and TA may also suggest that the astrophysics is not identical in both hemispheres. In that context, a composition-dependent anisotropy study will be of great interest. The promising aspect is that our measurements of air shower development, whether they be from FDs or SDs, are continuing to improve, with the likely future outcome being the ability to (at least) identify the lighter fraction of the flux with a surface detector, 24 hours per day, as being realized by AugerPrime.

Photon and neutrino limits set by the experiments have ruled out certain exotic production mechanisms for the highest-energy cosmic rays, including the decay of super-heavy dark matter. They are

now probing cosmogenic photon and neutrino models that may provide information on the fraction of protons present at the highest energies. Finally, measurements at the observatories are constraining some aspects of hadronic and nuclear interaction models at very high energy, a remarkable feat given the indirect view of the interactions afforded by characteristics of the air shower.

As well as these achievements, we have also discussed the present challenges for the field. For example, despite much progress in measurements at accelerators, and despite constraints from ultra-energetic cosmic rays, we do not know the systematic uncertainty to attach to a simulation prediction for the mean $X_{\rm max}$ of a proton (or any) shower, reducing the power of our mass measurements and their influence on the open astrophysics questions. It also means that we are currently limited in being able to confidently select showers initiated by low charge primaries in our attempts to improve the sensitivity to anisotropies, especially since we do not yet have a mass estimate for every event we observe. Finally, we still lack sufficient collecting area to answer some of the big questions, given that we appear to be faced with a cosmic ray sky remarkably free of strong anisotropies at the highest energies.

For the future, we must build on this impressive progress with new ideas and techniques that will lead to new observatories that are sufficiently large (and cost-effective) to answer the remaining questions. While further increases in collecting area are of prime importance, it seems crucial that future ground observatories be endowed with at least some mass-composition sensitivity for all collected events.

Acknowledgements

We thank all of our colleagues in the Pierre Auger and Telescope Array experiments for their inspiring collaboration. While we have benefitted greatly from discussions with many of them over the years, the responsibility for any errors in this article is entirely ours.

References

[1] J. F. Ormes. *Centenary Symposium 2012: Discovery of Cosmic Rays*, American Institute of Physics Conference Series (American Institute of Physics, Melville, New York, 2013), Vol. 1516.
[2] K.-H. Kampert and A. A. Watson, Eur. Phys. J. H **37**, 359 (2012) [arXiv:1207.4827] [physics.hist-ph]] [Search INSPIRE].
[3] M. Nagano and A. A. Watson, Rev. Mod. Phys. **72**, 689 (2000).
[4] J. Linsley, Proc. 8th Int. Cosmic Ray Conf., Jaipur (1963), Vol. 4, p. 77.
[5] H. R. Allan, R. F. W. Beamish, W. M. Glencross, D. M. Thomson, and R. D. Wills, Proc. Phys. Soc. London **79**, 1170 (1962).
[6] C. B. A. McCusker and M. M. Winn, Il Nuovo Cimento **28** 175 (1963).
[7] C. J. Bell et al., J. Phys. A. **7**, 990 (1974).
[8] T. A. Egorov et al., Recent results from Yakutsk experiment, In Proceedings of the Tokyo Workshop on Techniques for the Study of Extremely High Energy Cosmic Rays (Tokyo, September 27–30, 1993), p. 35.
[9] M. Nagano et al., J. Phys. G **10**, 1295 (1984).
[10] H. E. Bergeson et al., Phys. Rev. Lett. **39**, 847 (1977).
[11] R. M. Baltrusaitis, R. Cady, G. L. Cassiday, et al., Nucl. Instrum. Methods Phys. Res., Sect. A **240**, 410 (1985).
[12] G. Thomson, Nucl. Phys. B Proc. Suppl. **136**, 28 (2004).
[13] J. Abraham et al., Nucl. Instrum. Methods Phys. Res., Sect. A **523**, 50 (2004).
[14] P. Sokolsky and G. B. Thomson, J. Phys. G **34**, R401 (2007) [arXiv:0706.1248 [astro-ph]] [Search INSPIRE].
[15] R. U. Abbasi et al., Phys. Lett. B **619**, 271 (2005) [arXiv:astro-ph/0501317] [Search INSPIRE].
[16] R. U. Abbasi et al., Phys. Rev. Lett. **100**, 101101 (2008) [arXiv:astro-ph/0703099] [Search INSPIRE].

[17] J. Abraham et al., Phys. Rev. Lett. **101**, 061101 (2008) [arXiv:0806.4302 [astro-ph]] [Search INSPIRE].
[18] K. Greisen, Phys. Rev. Lett. **16**, 748 (1966).
[19] G. T. Zatsepin and V. A. Kuz'min, JETP Lett. **4**, 78 (1966).
[20] D. J. Bird et al., Phys. Rev. Lett. **71**, 3401 (1993).
[21] R. U. Abbasi et al., Phys. Rev. Lett. **104**, 161101 (2010) [arXiv:0910.4184 [astro-ph.HE]] [Search INSPIRE].
[22] R. U. Abbasi et al., Astropart. Phys. **32**, 53 (2009) [arXiv:0904.4500 [astro-ph.HE]] [Search INSPIRE].
[23] T. Abu-Zayyad et al., Phys. Rev. Lett. **84**, 4276 (2000) [arXiv:astro-ph/9911144] [Search INSPIRE].
[24] T. Abu-Zayyad et al., Astropart. Phys. **16**, 1 (2001) [arXiv:astro-ph/0008206].
[25] R. U. Abbasi et al., Astropart. Phys. **64**, 49 (2015) [arXiv:1408.1726 [astro-ph.HE]] [Search INSPIRE].
[26] J. Abraham et al., Phys. Rev. Lett. **104**, 091101 (2010) [arXiv:1002.0699 [astro-ph.HE]] [Search INSPIRE].
[27] A. Aab et al., Phys. Rev. D **90**, 122005 (2014).
[28] R. Engel, D. Heck, and T. Pierog, Annu. Rev. Nucl. Part. Science **61**, 467 (2011).
[29] D. d'Enterria, R. Engel, T. Pierog, S. Ostapchenko, and K. Werner, Astropart. Phys. **35**, 98 (2011) [arXiv:1101.5596 [astro-ph.HE]] [Search INSPIRE].
[30] A. Aab et al., Phys. Rev. D **90**, 122006 (2014).
[31] A. A. Ivanov, Astrophys. J. **804**, 122 (2015) [arXiv:1502.07496 [astro-ph.HE]] [Search INSPIRE].
[32] N. Chiba et al., Nucl. Instrum. Methods Phys. Res., Sect. A **311**, 338 (1992).
[33] K. Shinozaki, M. Teshima, and [AGASA Collaboration], Nucl. Phys. B Proc. Suppl. **136**, 18 (2004).
[34] M. Takeda et al., Astropart. Phys. **19**, 447 (2003) [arXiv:astro-ph/0209422] [Search INSPIRE].
[35] S. Yoshida and H. Dai, J. Phys. G **24**, 905 (1998) [arXiv:astro-ph/9802294] [Search INSPIRE].
[36] T. Abu-Zayyad et al., Nucl. Instrum. Methods Phys. Res., Sect. A **450**, 253 (2000).
[37] A. Aab et al., Nucl. Instrum. Methods Phys. Res., Sect. A **798**, 172 (2015).
[38] D. Ivanov et al., Proc. 34th Int. Cosmic Ray Conf., The Hague, Proc. of Science, ICRC2015, p. 349 (2016).
[39] A. A. Watson, Astropart. Phys. **53**, 107 (2014).
[40] P. Sommers, Astropart. Phys. **3**, 349 (1995).
[41] B. R. Dawson, H. Y. Dai, P. Sommers, and S. Yoshida, Astropart. Phys. **5**, 239 (1996).
[42] C. Bonifazi for [Pierre Auger Collaboration], Nucl. Phys. B Proc. Suppl. **190**, 20 (2009) [arXiv:0901.3138 [astro-ph.HE]] [Search INSPIRE].
[43] B. R. Dawson for [Pierre Auger Collaboration], Proc. 30th Int. Cosmic Ray Conf., Merida, Mexico (2007), Vol. 4, p. 425 [arXiv:0706.1105 [astro-ph]] [Search INSPIRE].
[44] A. Aab et al., J. Instrum. **12**, P02006 (2017).
[45] J. Abraham et al., Astropart. Phys. **33**, 108 (2010) [arXiv:1002.0366 [astro-ph.IM]] [Search INSPIRE].
[46] J. Blümer and [Pierre Auger Collaboration], New J. Phys. **12**, 035001 (2010).
[47] A. Aab et al., [arXiv:1604.03637 [astro-ph.IM]] [Search INSPIRE].
[48] S. Aiso et al. [Telescope Array Project], Proc. of the 25th Int. Cosmic Ray Conf., Durban (1997).
[49] Telescope Array Collaboration, Proc. of the 25th Int. Cosmic Ray Conf., Durban (1997).
[50] The TA collaboration, Telescope Array Technical Design Report (January 17, 2000) (available at: http://taws100.icrr.u-tokyo.ac.jp/documents/GenINFO/TA_TDR-20000117.pdf, date last accessed June 28, 2017).
[51] Y. Arai et al., Proc. of the 28th Int. Cosmic Ray Conf., Tsukuba, p. 1025 (2003).
[52] T. Abu-Zayyad et al., Nucl. Instrum. Methods Phys. Res., Sect. A **689**, 87 (2012) [arXiv:1201.4964 [astro-ph.IM]] [Search INSPIRE].
[53] H. Tokuno et al., Nucl. Instrum. Methods Phys. Res., Sect. A **676**, 54 (2012) [arXiv:1201.0002 [astro-ph.IM]] [Search INSPIRE].
[54] Y. Tameda et al., Nucl. Instrum. Methods Phys. Res., Sect. A **609**, 227 (2009).
[55] P. Tinyakov, Nucl. Instrum. Methods Phys. Res., Sect. A **742**, 29 (2014).
[56] T. Tomida et al., Nucl. Instrum. Methods Phys. Res., Sect. A **654**, 653 (2011).
[57] T. Tomida, M. Chikawa, M. Fukushima, et al., Atmospheric monitor for Telescope Array experiment, in *European Physical Journal Web of Conferences*, (2013) Vol. 53, p. 10003.
[58] Z. Zundel et al., Proc. 34th Int. Cosmic Ray Conf., The Hague, Proc. of Science, ICRC2015, p. 445 (2016).

[59] S. Kawana et al., Nucl. Instrum. Methods Phys. Res., Sect. A **681**, 68 (2012).
[60] B. K. Shin et al., Nucl. Instrum. Methods Phys. Res., Sect. A **768**, 96 (2014).
[61] H. Tokuno, Y. Murano, S. Kawana, et al., Nucl. Instrum. Methods Phys. Res., Sect. A **601**, 364 (2009).
[62] T. Shibata et al., Nucl. Instrum. Methods Phys. Res., Sect. A **597**, 61 (2008).
[63] B. Shin et al., Proc. 34th Int. Cosmic Ray Conf., The Hague, Proc. of Science, ICRC2015, p. 640 (2016).
[64] A. N. Bunner, *Cosmic Ray Detection by Atmospheric Fluorescence*, PhD thesis, Cornell University (1967).
[65] F. Kakimoto et al., Nucl. Instrum. Methods Phys. Res., Sect. A **372**, 527 (1996).
[66] M. Nagano, K. Kobayakawa, N. Sakaki, and K. Ando, Astropart. Phys. **22**, 235 (2004) [arXiv:astro-ph/0406474] [Search INSPIRE].
[67] M. Ave et al., Astropart. Phys. **42**, 90 (2013) [arXiv:1210.6734] [Search INSPIRE].
[68] C. C. Chen et al., Astropart. Phys. **25**, 129 (2006).
[69] V. Verzi for [Pierre Auger Collaboration], Proc. 33rd Int. Cosmic Ray Conf., Rio de Janeiro, (2013). (Available at: http://www.cbpf.br/∼icrc2013/papers/icrc2013-0928.pdf, date last accessed June 28, 2017.)
[70] D. Heck, J. Knapp, J. N. Capdevielle, G. Schatz, and T. Thouw, *CORSIKA: a Monte Carlo code to simulate extensive air showers*, Forschungszentrum Karlsruhe Report FZKA 6019 (1998).
[71] T. Bergmann, R. Engel, D. Heck, et al., Astropart. Phys. **26**, 420 (2007) [arXiv:astro-ph/0606564] [Search INSPIRE].
[72] T. Pierog, Iu. Karpenko, J. M. Katzy, E. Yatsenko, and K. Werner, Phys. Rev. C **92**, 034906 (2015) [arXiv:1306.0121 [hep-ph]] [Search INSPIRE].
[73] S. Ostapchenko, EPJ Web Conf. **52**, 02001 (2013).
[74] F. Riehn, R. Engel, A. Fedynitch, T. K. Gaisser, and T. Stanev, Proc. 34th Int. Cosmic Ray Conf., The Hague, Proc. of Science, ICRC2015, p. 558 (2016).
[75] T. Abu-Zayyad, R. Aida, M. Allen, et al., Astropart. Phys. **61**, 93 (2015) [arXiv:1305.7273 [astro-ph.HE]] [Search INSPIRE].
[76] I. Valino for [Pierre Auger Collaboration], Proc. 34th Int. Cosmic Ray Conf., The Hague, Proc. of Science, ICRC2015, p. 271 (2016).
[77] V. Berezinsky, A. Z. Gazizov, and S. I. Grigorieva, Phys. Lett. B **612**, 147 (2005).
[78] V. Verzi et al., Auger-TA energy spectrum working group report, in the International Conference UHECR 2016 (Kyoto, Japan, October 11-14, 2016). (Available at: https://indico.cern.ch/event/504078/contributions/2290831/, date last accessed June 28, 2017).
[79] V. Berezinsky, A. Gazizov, and S. Grigorieva, Phys. Rev. D **74**, 043005 (2006) [arXiv:hep-ph/0204357] [Search INSPIRE].
[80] V. Verzi, D. Ivanov, and Y. Tsunesada, Prog. Theor. Exp. Phys. **2017**, 12A103 (2017).
[81] E. Kido, O. Kalashev, et al., Proc. 34th Int. Cosmic Ray Conf., The Hague, Proc. of Science, ICRC2015, p. 258 (2016).
[82] A. di Matteo for [Pierre Auger Collaboration], Proc. 34th Int. Cosmic Ray Conf., The Hague, Proc. of Science, ICRC2015, p. 249 (2016).
[83] M. S. Pshirkov, P. G. Tinyakov, P. P. Kronberg, and K. J. Newton-McGee, Astrophys. J. **738**, 192 (2011).
[84] R. Jansson and G. R. Farrar, Astrophys. J. **757**, 14 (2012).
[85] I. Al Samarai for [Pierre Auger Collaboration], Proc. 34th Int. Cosmic Ray Conf., The Hague, Proc. of Science, ICRC2015, p. 372 (2016).
[86] D. M. Edge, A. M. T. Pollock, R. J. O. Reid, A. A. Watson, and J. G. Wilson, J. Phys. G **4**, 133 (1978).
[87] A. Aab et al., Astrophys. J. **802**, 111 (2015) [arXiv:1411.6953 [astro-ph.HE]] [Search INSPIRE].
[88] R. U. Abbasi et al., Astrophys. J. **790**, L21 (2014) [arXiv:1404.5890 [astro-ph.HE]] [Search INSPIRE].
[89] R. Aloisio, V. Berezinsky, and A. Gazizov, Astropart. Phys. **39-40**, 129 (2012).
[90] P. Abreu et al., Astrophys. J. Suppl. **203**, 34 (2012) [arXiv:1210.3736 [astro-ph.HE]] [Search INSPIRE].
[91] R. U. Abbasi et al., Astropart. Phys. **86**, 21 (2017) [arXiv:1608.06306 [astro-ph.HE]] [Search INSPIRE].
[92] A. Aab et al., Astrophys. J. **794**, 172 (2014) [arXiv:1409.3128 [astro-ph.HE]] [Search INSPIRE].
[93] O. Deligny for [Pierre Auger and Telescope Array Collaborations], Proc. 34th Int. Cosmic Ray Conf., The Hague, Proc. of Science, ICRC2015, p. 395 (2016).

[94] D. Allard, Astropart. Phys. **39**, 33 (2012) [arXiv:1111.3290 [astro-ph.HE]] [Search INSPIRE].
[95] A. Aab et al., Astrophys. J. **804**, 15 (2015) [arXiv:1411.6111 [astro-ph.HE]] [Search INSPIRE].
[96] T. Abu-Zayyad et al., Astrophys. J. **757**, 26 (2012) [arXiv:1205.5984 [astro-ph.HE]] [Search INSPIRE].
[97] T. Abu-Zayyad et al., Astrophys. J. **777**, 88 (2013) [arXiv:1306.5808 [astro-ph.HE]] [Search INSPIRE].
[98] P. Tinyakov for [Telescope Array Collaboration], TA anisotropy summary, in *Proc., UHECR 2016* (Kyoto, Japan, October 11-14, 2016). (in preparation 2016).
[99] P. Abreu et al., J. Cosmol. Astropart. Phys. **2013**, 009 (2013).
[100] J. Matthews, Astropart. Phys. **22**, 387 (2005).
[101] W. Hanlon et al. for [Telescope Array Collaboration], Composition measurements via depth of air shower maximum at the Telescope Array, in *Proc., UHECR 2016* (Kyoto, Japan, October 11-14, 2016). (in preparation 2016).
[102] R. U. Abbasi et al., Astropart. Phys. **64**, 49 (2015).
[103] A. Porcelli for [Pierre Auger Collaboration], Proc. 34th Int. Cosmic Ray Conf., The Hague, Proc. of Science, ICRC2015, p. 420 (2016).
[104] T. Stroman, Y. Tameda, et al., Proc. 34th Int. Cosmic Ray Conf., The Hague, Proc. of Science, ICRC2015, p. 361 (2016).
[105] E. Barcikowski, J. Bellido, J. Belz, et al., EPJ Web Conf., **53**, 01006 (2013) [arXiv:1306.4430 [astro-ph.HE]] [Search INSPIRE].
[106] R. Abbasi, J. Bellido, J. Belz, et al., Report of the working group on the composition of ultra high energy cosmic rays, In *Proc. Int. Symp. Ultra-High Energy Cosmic Rays (UHECR2014)* (Physical Society of Japan, 2016). (Available at: http://journals.jps.jp/doi/pdf/10.7566/JPSCP.9.010016, date last accessed June 28, 2017.)
[107] W. Hanlon et al. for [Pierre Auger collaboration and Telescope Array collaboration], Report of the working group on the mass composition of ultrahigh energy cosmic rays, in *Proc. UHECR 2016* (Kyoto, Japan, October 11-14, 2016). (in preparation in JPS Conf. Proc.).
[108] A. Aab et al., Phys. Rev. D **93**, 072006 (2016).
[109] A. Aab et al., Phys. Rev. D **90**, 012012 (2014) [arXiv:1407.5919 [hep-ex]] [Search INSPIRE].
[110] L. Collica for the Pierre Auger Collaboration, Eur. Phys. J. Plus **131**, 301 (2016) [arXiv:1609.02498 [astro-ph.HE]] [Search INSPIRE].
[111] A. Aab, P. Abreu, M. Aglietta, et al., Phys. Lett. B **762**, 288 (2016) [arXiv:1609.08567 [astro-ph.HE]] [Search INSPIRE].
[112] G. B. Gelmini, O. E. Kalashev, and D. V. Semikoz, J. Exp. Theor. Phys. **106**, 1061 (2008) [arXiv:astro-ph/0506128] [Search INSPIRE].
[113] B. Sarkar, K.-H. Kampert, et al., Proc. 32nd Int. Cosmic Ray Conf., Beijing, (2011) Vol. 2, p. 198.
[114] J. Ellis, V. E. Mayes, and D. V. Nanopoulos, Phys. Rev. D **74**, 115003 (2006) [arXiv:astro-ph/0512303] [Search INSPIRE].
[115] A. Aab, P. Abreu, M. Aglietta, et al., J. Cosmol. Astropart. Phys. **2017**, 009 (2017) [arXiv:1612.01517 [astro-ph.HE]] [Search INSPIRE].
[116] G. Rubtsov et al., Proc. 34th Int. Cosmic Ray Conf., The Hague, Proc. of Science, ICRC2015, p. 331 (2016).
[117] A. Aab et al., Phys. Rev. D **91**, 092008 (2015) [arXiv:1504.05397 [astro-ph.HE]] [Search INSPIRE].
[118] G. I. Rubtsov, M. Fukushima, D. Ivanov, et al., Search for ultra-high energy photons and neutrinos using Telescope Array surface detector, in *European Physical Journal Web of Conferences*, (2013) Vol. 53, p. 05001.
[119] C. Bleve for [Pierre Auger Collaboration], Proc. 34th Int. Cosmic Ray Conf., The Hague, Proc. of Science, ICRC2015, p. 1103 (2016).
[120] M. G. Aartsen et al., Phys. Rev. Lett. **117**, 241101 (2016) [arXiv:1607.05886 [astro-ph.HE]] [Search INSPIRE].
[121] [IceCube Collaboration], [Pierre Auger Collaboration], and [Telescope Array Collaboration], J. Cosmol. Astropart. Phys. **1**, 037 (2016) [arXiv:1511.09408 [astro-ph.HE]] [Search INSPIRE].
[122] A. Aab et al., Phys. Rev. D **94**, 122007 (2016) [arXiv:1608.07378] [Search INSPIRE].
[123] M. Honda, M. Nagano, S. Tonwar, K. Kasahara, T. Hara, N. Hayashida, Y. Matsubara, M. Teshima, and S. Yoshida, Phys. Rev. Lett. **70**, 525 (1993).

[124] R. M. Baltrusaitis, G. L. Cassiday, J. W. Elbert, P. R. Gerhardy, S. Ko, E. C. Loh, Y. Mizumoto, P. Sokolsky, and D. Steck, Phys. Rev. Lett. **52**, 1380 (1984).
[125] R. W. Ellsworth, T. K. Gaisser, T. Stanev, and G. B. Yodh, Phys. Rev. D **26**, 336 (1982).
[126] K. Belov et al., Nuclear Phys. B **151**, 197 (2006).
[127] P. Abreu et al., Phys. Rev. Lett. **109**, 062002 (2012) [arXiv:1208.1520 [hep-ex]] [Search INSPIRE].
[128] R. Ulrich for [Pierre Auger Collaboration], Proc. 34th Int. Cosmic Ray Conf., The Hague, Proc. of Science, ICRC2015, p. 401 (2016).
[129] R. U. Abbasi et al., Phys. Rev. D **92**, 032007 (2015) [arXiv:1505.01860 [astro-ph.HE]] [Search INSPIRE].
[130] T. Abu-Zayyad et al., Astrophys. J. Lett. **768**, L1 (2013) [arXiv:1205.5067 [astro-ph.HE]] [Search INSPIRE].
[131] A. Aab et al., Phys. Rev. D **91**, 059901 (2015).
[132] A. Aab et al., Phys. Rev. Lett. **117**, 192001 (2016).
[133] R. Takeishi, *Study of muons from ultra-high energy cosmic ray air showers measured with the Telescope Array experiment*, PhD thesis, University of Tokyo (2017).
[134] J. Linsley, Int. Cosmic Ray Conf., (1977) Vol. 12, p. 89.
[135] R. U. Abbasi et al., Astrophys. J. **622**, 910 (2005).
[136] J. L. Puget, F. W. Stecker, and J. H. Bredekamp, Astrophys. J. **205**, 638 (1976).
[137] F. W. Stecker and M. H. Salamon, Astrophys. J. **512**, 521 (1999) [arXiv:astro-ph/9808110] [Search INSPIRE].
[138] A. Aab et al., J. Cosmol. Astropart. Phys. **2017**, 038 (2017) [arXiv:1612.07155 [astro-ph.HE]] [Search INSPIRE].
[139] A. M. Taylor, *The propagation of ultra high energy cosmic rays*, PhD thesis, University of Oxford (2007). (Available at: https://ora.ox.ac.uk/objects/uuid:63572ebe-fb32-41b6-8b91-a7294db135a6, date last accessed June 28, 2017).
[140] D. Hooper, S. Sarkar, and A. M. Taylor, Phys. Rev. D **77**, 103007 (2008) [arXiv:0802.1538 [astro-ph]] [Search INSPIRE].
[141] A. De Cia et al., Astron. Astrophys. **596**, A97 (2016) [arXiv:1608.08621] [Search INSPIRE].
[142] J.-K. Krogager, J. P. U. Fynbo, P. Noterdaeme, T. Zafar, P. Møller, C. Ledoux, T. Krühler, A. Stockton, Mon. Not. R. Astron. Soc. **455**, 2698 (2016) [arXiv:1510.04695 [astro-ph.GA]] [Search INSPIRE].
[143] H. Gail, Condensation of dust in astrophysical environments, in *Laboratory Astrochemistry: From Molecules to Nanoparticles to Grains*, eds. S. Schlemmer, T. Giesen, C. Jager, and H. Mutschke (John Wiley & Sons, Inc., Hoboken, NJ, 2015).
[144] C. Song, Z. Cao, B. R. Dawson, et al., Astropart. Phys. **14**, 7 (2000) [arXiv:astro-ph/9910195] [Search INSPIRE].
[145] T. Huege, Radio detection of cosmic rays - achievements and future potential, in Proc. UHECR 2016 (Kyoto, Japan, October 11-14, 2016). (in preparation in JPS Conf. Proc.).
[146] S. Buitink et al., Phys. Rev. D **90**, 082003 (2014) [arXiv:1408.7001 [astro-ph.IM]] [Search INSPIRE].
[147] P. Abreu et al., J. Instrum. **7**, P10011 (2012).
[148] A. Aab et al., Phys. Rev. D **93**, 122005 (2016).
[149] T. Huege, Phys. Rep. https://doi.org/10.1016/j.physrep.2016.02.001**620**, 1 (2016).
[150] V. Verzi, Proc. 34th Int. Cosmic Ray Conf., The Hague, Proc. of Science, ICRC2015, p. 015 (2016).
[151] M. Ave et al., Nucl. Instrum. Methods Phys. Res., Sect. A **597**, 41 (2008).
[152] R. Abbasi et al., Nucl. Instrum. Methods Phys. Res., Sect. A **597**, 37 (2008).
[153] R. Abbasi et al., Astropart. Phys. **29**, 77 (2008) [arXiv:0708.3116] [Search INSPIRE].
[154] R. Abbasi, T. Abu-Zayyad, K. Belov, et al., Nucl. Instrum. Methods Phys. Res., Sect. A **597**, 32 (2008).
[155] P. Colin et al., Astropart. Phys. **27**, 317 (2007) [arXiv:astro-ph/0612110] [Search INSPIRE].
[156] J. Abraham et al., Science **318**, 938 (2007) [arXiv:0711.2256 [astro-ph]] [Search INSPIRE].
[157] D. N. Pfeffer, E. D. Kovetz, and M. Kamionkowski, Mon. Not. R. Astron. Soc. **466**, 2922 (2017) [arXiv:1512.04959 [astro-ph.HE]] [Search INSPIRE].
[158] H.-N. He, A. Kusenko, S. Nagataki, B.-B. Zhang, R.-Z. Yang, and Y.-Z. Fan, Phys. Rev. D **93**, 043011 (2016) [arXiv:1411.5273 [astro-ph.HE]] [Search INSPIRE].
[159] H. Sagawa and [Telescope Array Collaboration], Proc. 34th Int. Cosmic Ray Conf., The Hague, Proc. of Science, ICRC2015, p. 657 (2016).
[160] E. Kido for [Telescope Array Collaboration], The TAx4 experiment, in Proc. UHECR 2016 (Kyoto, Japan, October 11-14, 2016). (in preparation in JPS Conf. Proc.).

[161] P. Lipari, Phys. Rev. D **79**, 063001 (2009) [arXiv:0809.0190 [astro-ph]] [Search INSPIRE].
[162] T. Okuda et al., Proc. 34th Int. Cosmic Ray Conf., The Hague, Proc. of Science, ICRC2015, p. 298 (2016).
[163] J. Belz et al. for [Telescope Array and TA/LMA collaborations], High-energy particle showers observed at ground level in coincidence with downward lightning leaders at the Telescope Array Observatory, in Proc. UHECR 2016 (Kyoto, Japan, October 11-14, 2016). (in preparation in JPS Conf. Proc.).
[164] A. Tonachini for [Pierre Auger Collaboration], Proc. 33rd Int. Cosmic Ray Conf., Rio de Janeiro, (2013). (Available at: http://www.cbpf.br/ icrc2013/papers/icrc2013-0676.pdf.)
[165] R. Colalillo for [Pierre Auger collaboration], Elves, Forbush decreases and solar activity studies at the Pierre Auger observatory, in Proc. UHECR 2016 (Kyoto, Japan, October 11-14, 2016). (in preparation in JPS Conf. Proc.).
[166] S. Buitink et al., Astron. Astrophys. **467**, 385 (2007).
[167] T. Huege, Phys. Rep. **620**, 1 (2016).
[168] P. W. Gorham et al., Phys. Rev. Lett. **103**, 051103 (2009).
[169] P. Allison et al. [The ARA collaboration], Phys. Rev. D **93**, 082003 (2016).
[170] S. W. Barwick et al., Astropart. Phys. **90**, 50 (2017).
[171] P. W. Gorham et al., Phys. Rev. D **78**, 032007 (2008).
[172] R. Smida et al., Phys. Rev. Lett. **113**, 221101 (2014).
[173] I. S. Ohta et al., Nucl. Instrum. Methods Phys. Res., Sect. A **810**, 44 (2016).
[174] R. U. Abbasi et al., Astropart. Phys. **87**, 1 (2017) [arXiv:1603.05217 [astro-ph.IM]] [Search INSPIRE].
[175] L. Scarsi et al., EUSO - Extreme Universe Space Observatory, in Proc. 27th Int. Cosmic Ray Conf. (Hamburg, HE, 2001), pp. 839–842.
[176] J. H. Adams et al., Astropart. Phys. **44**, 76 (2013).
[177] J. H. Adams et al., Exp. Astron. **40**, 183 (2015).
[178] M. Casolino for [JEM-EUSO collaboration], The JEM-EUSO program to study UHECR from space, in Proc. UHECR 2016 (Kyoto, Japan, October 11-14, 2016). (in preparation in JPS Conf. Proc.).
[179] M. Zotov for [Lomonosov-UHECR/TLE collaboration], Early results from TUS, the first orbital detector of extreme energy cosmic rays, in Proc. UHECR 2016 (Kyoto, Japan, October 11-14, 2016). (in preparation in JPS Conf. Proc.).
[180] R. Aloisio, V. Berezinsky, P. Blasi, A. Gazizovc, S. Grigorievad, and B. Hnatyk, Astropart. Phys. **27**, 76 (2007) [arXiv:astro-ph/0608219] [Search INSPIRE].
[181] T. Fujii et al., Astropart. Phys. **74**, 64 (2016).
[182] Y. Tameda et al., Development of the cosmic ray air fluorescence Fresnel lens telescope for a next generation UHECR observatory, in Proc. UHECR 2016 (Kyoto, Japan, October 11-14, 2016). (in preparation in JPS Conf. Proc.).
[183] K. Hashimoto, K. Honda, N. Kawasumi, et al., Performance test of leadburger: Detector for measurement of highest energy cosmic rays, in *Proc. 24th Int. Cosmic Ray Conf. Rome* (1995).
[184] K. Honda, K. Hashimoto, N. Kawasumi, T. Kutter, M. Nagano, and I. Tsushima, Phys. Rev. D **56**, 3833 (1997).
[185] A. Anastasio et al., Nucl. Instrum. Methods Phys. Res., Sect. A **718**, 134 (2013).
[186] T. Nonaka et al. for [Telescope Array Collaboration], Muon detector R&D in Telescope Array experiment, in *Proc. UHECR 2014, Springdale, USA, October 12-15, 2014*, JPS Conf. Proc., (2016) Vol. 9, p. 010013.
[187] C. Peters et al., Prospects of silicon photomultipliers for ground-based cosmic ray experiments, in Proc. UHECR 2016 (Kyoto, Japan, October 11-14, 2016). (in preparation in JPS Conf. Proc.).